***N*^{o} d'ordre:**

Université Kasdi Merbah Ouargla

Faculté des Mathématiques et Sciences de la Matière

Département de Physique

Thèse de Doctorat

Présentée pour l'obtention du grade de **Docteur**

En : Physique

Spécialité : Rayonnement et Matière

Par : Hadda GOSSA

Thème

Contribution of relativistic Doppler broadening to spectral lines in plasma

Soutenue publiquement, le **09/01/2024**, devant le jury composé de :

Mr.	F. Khelfaoui	Pr	Université Kasdi Merbah Ouargla	Président
Mr.	M.T. Meftah	Pr	Université Kasdi Merbah Ouargla	Rapporteur de thèse
Mr.	S. Douis	Pr	Université Kasdi Merbah Ouargla	Examinateur
Mrs.	K. Chenini	Pr	Université de Ghardaia	Examinateur
Mr.	A. Kaddour	Pr	URAER Ghardaia	Examinateur
Mr.	L. Benmebrouk	Pr	Université Kasdi Merbah Ouargla	Examinateur

***N*^{o} d'ordre:**

Université Kasdi Merbah Ouargla

Faculté des Mathématiques et Sciences de la Matière

Département de Physique

Thèse de Doctorat

Présentée pour l'obtention du grade de **Docteur**

En : Physique

Spécialité : Rayonnement et Matière

Par : Hadda GOSSA

Thème

Contribution de l'élargissement Doppler relativiste aux raies spectrales dans les plasmas

Soutenue publiquement, le **09/01/2024**, devant le jury composé de :

Mr.	F. Khelfaoui	Pr	Université Kasdi Merbah Ouargla	Président
Mr.	M.T. Meftah	Pr	Université Kasdi Merbah Ouargla	Rapporteur de thèse
Mr.	S. Douis	Pr	Université Kasdi Merbah Ouargla	Examinateur
Mrs.	K. Chenini	Pr	Université de Ghardaia	Examinateur
Mr.	A. Kaddour	Pr	URAER Ghardaia	Examinateur
Mr.	L. Benmebrouk	Pr	Université Kasdi Merbah Ouargla	Examinateur

To my dear mother, who stayed up tired
and praying to God for this moment, perhaps
even more fervently than I did
to my soulful father
to my dear husband and soulmate
to my dear brothers and sisters
and to all my family and cherished friends

Acknowledgements

Praise be to the God who has given me faith, courage, and patience to carry out this work.

I would like to express my heartfelt gratitude to the following individuals and institutions who have been instrumental in the process of finishing my PhD thesis:

My heartfelt gratitude to my supervisor, Pr. Mohammed Tayeb MEFTAH, for the trust he has placed in me, through his constant presence, modesty, advice, great scientific qualities, patience, invaluable assistance, and constructive remarks for the good progress of this work.

The members of my doctoral committee, including Professor Fethi KhELFAOUI (University of Ouargla), who served as the President of the committee, Professor Saïd DOUIS (University of Ouargla), Professor Keltoum CHENINI (University of Ghardaïa), Pr. Abdelmadjid KADDOUR (URAER Ghardaïa), and Professor Lazhar BENMEBROUK (University de Ouargla), who served as Examiners. I am grateful for their invaluable feedback, critical evaluation, and scholarly contributions.

I extend my sincere gratitude to the Laboratory RPPS for their invaluable support and resources throughout this research endeavor.

The faculty and staff of the Physics Department at Kasdi Merbah Ourgla University, for providing a stimulating academic environment, access to resources, and opportunities for intellectual growth. I am grateful for the invaluable knowledge and skills I have gained through their teaching, mentorship, and collaboration.

The research participants who generously contributed their time, expertise, and valuable insights to this study. Without their willingness to participate, this research would not have been possible. I am deeply grateful for their contributions and trust.

I express my deep gratitude to my mother for her prayers, patience, and invaluable encouragement.

My family and friends, for their unwavering support, encouragement, and belief in my abilities. Their love, understanding, and patience have been a constant source of strength throughout this demanding journey. I am truly grateful for their presence in my life.

Colleagues and fellow researchers, for their stimulating discussions, collaboration, and shared experiences.

I am grateful to the many contributors, including individuals, institutions, and funding agencies, whose groundbreaking research and support have shaped my work and advanced knowledge in my field.

ملخص

في هذا العمل ركزنا اهتمامنا على تأثير الحالة النسبية على الخط الطيفي الناتج عن فعل دوبلر الشهير ومساهمته في الخطوط الطيفية في البلازما. ولهذا بداية أبرزنا أهمية دراسة الخطوط الطيفية في البلازما، ثم أهمية هذا الخط الطيفي بالخصوص، حيث قدمنا عبارة الخط الطيفي الناتج عن فعل دوبلر المعروف في الحالة الكلاسيكية، ثم انتقلنا الى جوهر هذه الدراسة بتقديم عبارة جديدة لكل من الخط الطيفي لتوسيع دوبلر النسبي أين وجدناه يعرض لنا عدم تناظر، بحيث يختلف عن الكلاسيكي المعروف بشكله الغاوسي المتناظر وتوسيع الخط الطيفي عند المنتصف الناتج عنه في الحالة النسبية، وهي مختلفة تماما عن العبارة المعروفة في الحالة الكلاسيكية، أين استخدمنا توزيع جيتنر-ماكسويل للسرعات بدل توزيع ماكسويل المستخدم في العبارة الكلاسيكية. كما قمنا بحساب التوسيع من أجل أيونات لأشباه الهيدروجين في درجات حرارة عالية، وعمل مقارنة بين توسيع دوبلر في الحالتين (النسبية والكلاسيكية) أين وجدنا أنهما متقاربان جدا، ولكن هذا التقارب يبتعد بزيادة درجة الحرارة ومنه وجب أخذ الحالة النسبية بعين الاعتبار. كما أضفنا مقارنة بين توسيع دوبلر وتوسيع ستارك الذي يعتبر وتوسيع دوبلر من أهم التوسيعات في الخطوط الطيفية في البلازما. لقد وجدنا أن توسيع دوبلر هو الغالب في الحالة النسبية إلا أنه يجب أخذ توسيع ستارك بعين الاعتبار وعدم إهماله في الكثافات العالية جدا، كما أرفقنا هذا العمل أيضا بمقارنات تجريبية من أجل جعل هذه الدراسة موضوعية.

الكلمات المفتاحية: الخطوط الطيفية، فعل دوبلر، فعل دوبلر النسبي، تعريض دوبلر، توزيع جيتنر-ماكسويل، تعريض ستارك.

Abstract

In this work, we have essentially focused on the effect of the relativistic Doppler broadening and its contribution to spectral lines in plasma. For that reason, the importance was first given to the study of the spectral lines in plasma as well as the importance of that broadening. Secondly, and with the study development, a new formula for Doppler broadening in the relativistic case was attained due to the relativistic Doppler effect by using the Maxwell-Jüttner distribution. According to the latter, it was found that it not have a Gaussian profile not like the classical (non-relativistic) Doppler broadening. Moreover, evidence indicates that in the realm of relativity, the spectral line profile displays an asymmetry due to the Doppler broadening. Furthermore, a novel Full Width at Half Maximum (FWHM) formula for the corresponding profile, distinct from the commonly known classical formula, has also been derived. In addition, the FWHM of some hydrogen-like ions in ultra-high-temperature (using the relativistic FWHM formula) was also calculated. Besides that, a comparison of the relativistic and classical Doppler broadening was done. It has been found that there is not much difference between them, but when temperature increases the difference increases. Consequently, the relativistic case must be taken into account. In addition to those previously mentioned, a comparison between Doppler broadening and Stark broadening was added. This is considered and the Doppler broadening is one of the most important broadening in spectral lines in plasma. It was found that Doppler broadening is always predominant in the relativistic case, but that Stark broadening should be taken into account or not neglected at very high densities. It should be noted that this work is backed by experimental comparisons.

Keywords: spectral lines broadening, Doppler effect, relativistic Doppler effect, Doppler broadening, Maxwell-Jüttner distribution, Stark broadening.

Abstract

Dans ce travail, nous nous sommes concentrés sur l'effet de l'élargissement Doppler relativiste et sa contribution aux raies spectrales dans le plasma. Pour cette raison, nous avons d'abord souligné l'importance d'étudier les raies spectrales dans le plasma et l'impact de cet élargissement. Ensuite, nous avons introduit une nouvelle formule pour l'élargissement Doppler dans le cas relativiste, utilisant la distribution de Maxwell-Jüttner, et avons constaté qu'elle ne produit pas de profil gaussien contrairement à l'élargissement Doppler non relativiste. De plus, nous avons observé une asymétrie dans le profil de raie spectrale due à l'élargissement Doppler relativiste. Nous avons également dérivé une nouvelle formule FWHM du profil correspondant, différente de la formule classique. Nous avons également calculé le FWHM (Pleine Largeur à Mi-Hauteur) de certains ions hydrogénoïdes à ultra-haute température (en utilisant la formule FWHM relativiste) et avons comparé l'élargissement Doppler classique et relativiste, constatant une différence minimale qui augmente avec la température, soulignant l'importance du cas relativiste. Nous avons également comparé l'élargissement Doppler et Stark, confirmant la prédominance de l'élargissement Doppler dans le cas relativiste, mais reconnaissant l'importance de l'élargissement Stark à très fortes densités. Des comparaisons expérimentales appuient nos résultats.

Mots Clés: élargissement des raies spectrales, effet Doppler, effet Doppler relativiste, élargissement Doppler, distribution Maxwell-Jüttner, élargissement Stark.

Contents

List of Figures

List of Tables

General Introduction

One of the most crucial diagnostic tools involves the analysis of radiation emitted in plasma, leading to the development of plasma spectroscopy [1–9]. The movement of ions, neutral atoms, or molecules within the plasma is akin to mobile antennae [3, 10].
This study explores phenomena such as ionization, absorption, excitation, recombination, and de-excitation that characterize emitter plasma behavior. The emitted plasma radiation encapsulates not only interactions between emitters (atoms or ions) and their surroundings but also their dynamic behavior, including the Doppler effect, observable as line profiles of emission lines.

The dynamics and interactions of emitters are orchestrated by spectral lines, which are broadened, shifted, and deformed, rejecting the notion of infinitesimal spectral widths. Interactions between emitters and surrounding particles, particularly ions, have been extensively studied and continue to evolve [1, 11–17]. Other contributing factors include the dynamics or movement of emitters, translating into the Doppler effect.

The study of spectral line shapes, incorporating both broadening and shifts, holds fundamental and practical importance, serving as a potent diagnostic tool across various media, including magnetically confined fusion plasmas, laser-produced plasmas, astrophysical plasmas, and planetary atmospheres [1].

The overall width of a spectral line is dictated by the interplay of various broadening mechanisms, incorporating natural line broadening, instrumental line broadening, Doppler broadening, electron impact broadening, and Stark broadening. Each of these mechanisms plays a role in shaping the line, contributing to its comprehensive width. Specifically, Doppler broadening and Stark broadening, induced by collisions, pose computational challenges when quantifying their impact on line broadening. These intricacies, coupled with factors such as natural and experimental broadening, necessitate meticulous consideration and inclusion in computational models or analyses of spectral line profiles. Understanding the combined influence of these mechanisms is pivotal for accurate interpretations and predictions in the study of spectral lines [18].

Under specific conditions of temperature or density, a particular broadening effect

tends to overshadow others. The prevalence of a specific broadening mechanism is contingent upon the local plasma temperature and density. The other mechanisms are generally viewed as minor adjustments to the dominant one, given their comparatively smaller contributions to the overall broadening [3].

In some cases, it is more appropriate to take two broadening into account for example, in the range of temperatures from ($2 \times 10^4 - 5 \times 10^5$ K), and for an electron density of $n_e = 10^{17} cm^{-3}$ [19], the stark broadening mechanism is dominant, comparable to the Doppler broadening. But when temperatures increase, and in the range of it from 50 eV to 400 eV ($5.8 \times 10^5 - 4.6 \times 10^5$ K) and for an electron density ranged from $n_e = 10^{18} cm^{-3}$ to $n_e = 10^{24} cm^{-3}$, the stark broadening still dominant, but we have to be taken the Doppler broadening into account [12].

Doppler broadening, often referred to as thermal broadening, is a phenomenon rooted in the Doppler effect, a renowned principle in physics and a pivotal factor in various fields such as plasma studies and astronomy. First identified by the scientist Christian Doppler in the 19th century, the Doppler effect occurs when the frequency of a wave changes due to the relative motion between its source and the observer, impacting both its period and wavelength. This effect is not confined to a specific type of wave and affects both electromagnetic and mechanical waves.

In the context of spectral lines, Doppler broadening manifests as a consequence of the Doppler effect experienced by atoms or ions. Substantial research has been dedicated to comprehending and illustrating the Doppler effect, leading to significant advancements like the generalized relativistic Doppler effect. These developments have garnered considerable attention in recent decades, indicating the persistent interest in refining our understanding of this phenomenon.

U. Fantz's work is illustrative of the practical applications of Doppler broadening [20], his research highlights how Doppler broadening can be a valuable tool for deducing gas temperature, particularly when it stands as the primary mechanism influencing line broadening. This underscores the versatility and importance of Doppler broadening as a diagnostic tool, showcasing its utility in determining key parameters in various scientific investigations.

Sun Mi Chung et al. [21], and J. S. Wark et al. [22] have conducted extensive investigations into the shift, broadening, and structure of X-ray emission emanating from an ALGOL star and laser-produced plasmas, respectively. These studies offer valuable insights into the unique characteristics of X-ray emissions within these specific systems, enhancing our understanding of their intricate dynamics.

In addition, Z. Simic has undertaken a detailed comparison between Stark broadening and Doppler broadening in the context of a Cd I plasma [23]. The findings from this

analysis highlight that, in this specific case, Doppler broadening plays a relatively minor role compared to the significant impact of Stark broadening.

N.I. Kosarev explored the influence of the Doppler effect on radiative transfer in moving plasma [24]. Furthermore, K. Fujii et al. [25], and Shinohara et al. [26] demonstrated the presence of Doppler broadening in the observable emission line of highly charged ions of tungsten at a wavelength of 668.899nm ($\lambda_0 = 668.899nm$).

Yuan-Pei Yang et al. [27], utilized the Doppler effect observed from astronomical objects to scrutinize the validity of the special theory of relativity.

Numerous other researchers have made substantial contributions to this field of study, profoundly influenced by the Doppler effect. Collectively, these investigations deepen our understanding of the multifaceted role played by Doppler broadening in diverse physical systems, ranging from astrophysical phenomena to laboratory-produced plasma.

In the realm of relativistic physics, electrons exhibit relative velocities, prompting the calculation of the relativistic electron collision operator, particularly pertinent in scenarios like fusion plasma, astrophysics, and laser technology where temperatures span from ($10^8 \leq T \leq 10^{11}$ K) [28]. In this temperature range, the relativistic effects become significant, leading to the dominance of the Doppler effect, a departure from classical expectations.

This study's primary objective is to introduce the formulation of the classical Doppler effect in the context of line profile broadening. A more intricate derivation is presented to articulate accurate expressions for both classical and relativistic Doppler effects influencing spectral line broadening observed in plasma. The classical Doppler Effect relies on the Maxwell velocity distribution to characterize emitters. However, practical constraints of the Maxwell distribution prompt the application of the relativistic Maxwell-Jüttner distribution in the relativistic Doppler Effect. This distribution is notably relevant in scenarios involving very high temperatures ranging from ($10^8 \leq T \leq 10^{11}$ K), as seen in fusion plasma, astrophysics, cosmology (primordial Universe), and experiments involving unstable Z Pinch configurations [28]. Importantly, the Juttner-Maxwell distribution is more general than the Maxwell distribution.

Crucially, the formulated approach maintains its validity across all temperature ranges, describing the relativistic particle velocity distribution applicable in diverse scenarios, spanning both low and high temperatures. The study concludes with a comparative analysis of various phenomena, providing a comprehensive understanding of the nuanced effects of Doppler broadening in different temperature regimes.

This project is organized into three chapters, each addressing distinct facets of plasma physics. The initial chapter delves into a comprehensive exploration of plasma principles, emphasizing the critical role played by parameters such as temperature and charge den-

sity in classifying different plasma types. This detailed examination serves to elucidate how variations in these parameters contribute to the distinctive characteristics exhibited by various plasmas. Furthermore, the chapter delves into an in-depth analysis of line broadening phenomena, recognizing that an understanding of line shapes is paramount for effective diagnostics in both laboratory and space plasma environments. This exploration aims to provide a nuanced perspective on the intricate interplay between plasma properties and line broadening, enhancing our comprehension of the diverse behaviors exhibited by different types of plasma in varied settings.

In the second chapter, we will delve into the classical Doppler broadening, specifically exploring the non-relativistic case governed by the classical Doppler Effect. As part of this exploration, we will introduce and derive the well-established formula for the classical Full Width at Half Maximum (FWHM) that characterizes the corresponding classical profile.

Moreover, our focus will shift towards the derivation of a novel expression for relativistic Doppler broadening, accounting for the potentially high velocities exhibited by the emitters in the relativistic scenario. This endeavor requires us to incorporate a suitable velocity distribution for the emitters, enabling the formulation of a new Full Width at Half Maximum (FWHM) formula meticulously designed to capture the nuances of the relativistic case. Through this detailed examination, we aim to provide a comprehensive understanding of both classical and relativistic Doppler broadening, shedding light on their distinct characteristics and implications in various physical scenarios.

The apex of this study is encapsulated in the third chapter, where a thorough examination unfolds, presenting several relativistic effects influencing spectral line broadening. Additionally, the chapter offers detailed comparisons involving distinct hydrogen-like species and varying temperatures of the Lyman-alpha line. Numerical results and discussions further enrich this analysis. Furthermore, a concise comparison between Doppler broadening and Stark broadening is presented, encompassing both classical and relativistic scenarios. This segment elucidates the nuanced similarities and differences between these two broadening mechanisms, delving into their respective impacts on line profiles across diverse scenarios. The chapter serves as a comprehensive exploration of relativistic effects, offering valuable insights into the distinctive contributions of Doppler and Stark broadening in shaping spectral features under various conditions.

The conclusion of the entire work, offering a condensed overview of the key findings, implications, and contributions of the research. This section provides a brief recapitulation of the primary results obtained throughout the study, highlighting the significance of these findings within the broader scope of plasma physics or related fields. Furthermore, it may propose potential directions for further research or applications based on the drawn conclusions, contributing to the comprehensive closure of the research endeavor.

Chapter 1

Theory of spectral lines broadening in plasma

1.1 Introduction

The initiation into the theory of spectral lines broadening in plasma takes us on a mesmerizing expedition through the complexities of astrophysics and plasma physics. Here, the conduct of matter under extreme conditions unfolds in a spectacular array of phenomena. Spectral lines, acting as distinctive imprints of atoms and ions emitting or absorbing light at specific wavelengths, emerge as invaluable tools for probing the characteristics and circumstances of astrophysical plasmas.

Within the expansive realms of the cosmos, plasmas assume a fundamental role, standing as the predominant state of matter in celestial bodies such as stars, galaxies, and interstellar mediums. Grasping the spectral lines emitted by these plasmas becomes pivotal in unraveling the enigmas surrounding their composition, temperature, density, and magnetic fields.

The theory of spectral lines broadening in plasma scrutinizes the mechanisms causing the once sharp and well-defined spectral lines to broaden or shift. A primary contributor to this broadening is the Doppler effect, stemming from the thermal motion of particles within the plasma. The varying velocities of charged particles induce shifts in the frequency of emitted radiation, leading to line broadening that unveils insights into the plasma's temperature.

Furthermore, the interplay between charged particles and the surrounding electric and magnetic fields introduces additional mechanisms for broadening. The Stark effect, prompted by electric fields, and the Zeeman effect, triggered by magnetic fields, add layers of complexity to the spectral lines, enabling scientists to deduce the strength and structure

of these fields within plasmas.

Whether in laboratory plasmas or astrophysical settings, comprehending spectral line broadening is indispensable for interpreting observational data and gaining profound insights into the underlying physical processes. The applications of this theory span various domains, from diagnosing conditions within distant stars to optimizing controlled fusion experiments on earth.

As we embark on this expedition through the theory of spectral lines broadening in plasma, we unveil a portal to the core of celestial bodies. Here, the intricate interplay between charged particles and electromagnetic forces orchestrates a symphony of light, holding the key to unlocking the secrets of the universe. In this chapter, our exploration commences with a succinct introduction to the captivating realm of plasma and its fundamental properties. Before delving into the intricate details surrounding the reasons behind spectral lines, it is essential to establish a foundational understanding of what plasma entails and the distinctive characteristics that define its behavior. Plasma, often referred to as the fourth state of matter, exhibits unique properties that distinguish it from solids, liquids, and gases.

As we embark on this introductory journey, we will elucidate the basic concepts underlying plasma physics, addressing key features such as ionization, temperature, and density. This foundational knowledge will lay the groundwork for a comprehensive exploration into the intricate mechanisms contributing to the formation of spectral lines. By understanding the inherent nature of plasma, we aim to enrich our appreciation for the profound role it plays in generating the diverse and informative spectral signatures that hold valuable diagnostic insights.

1.2 Plasma

Plasma physics constitutes the exploration of matter in a distinct state characterized by charged particles, commonly referred to as the fourth state of matter due to its unique properties setting it apart from solids, liquids, and gases. The formation of plasma typically occurs through the heating of gas until electrons detach from their parent atoms or molecules. Over the past few years, plasma physics has gained considerable significance, particularly in unraveling the mysteries of our universe, with claims that approximately 99% of the universe's matter exists in the plasma state. Within this context, plasma diagnostics encompass a diverse array of methods and experimental techniques aimed at measuring various plasma properties, including density, temperature, spatial profiles, and dynamics. These diagnostic tools play a crucial role in deriving essential plasma

parameters [2].

1.2.1 Classification of plasma

A plasma exhibits numerous defining features, including temperature, degree of ionization, and density, which collectively contribute to its classification into distinct states. These states can be delineated based on their coordinates in a plot of electron temperature kT_e vs n_e, as depicted in Figure (1.1). This graphical representation allows for the differentiation of various plasmas, each characterized by its unique thermal motion of electrons and electron density n_e. The diverse positions of plasmas on this plot provide a comprehensive framework for understanding their distinct behaviors and properties within the broader realm of plasma physics [5].

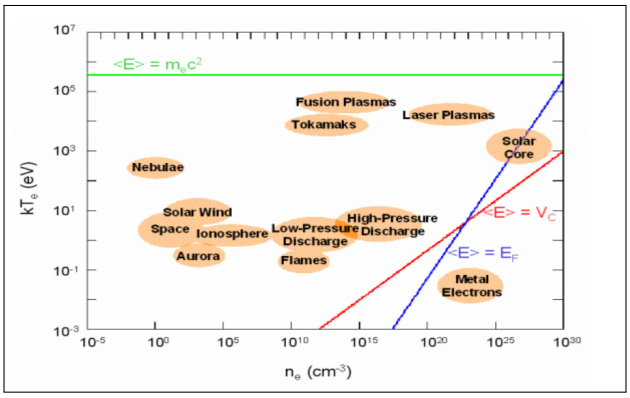

Fig 1.1: Classification of plasma.

In Figure (1.1), the condition where $kT_e \geqslant 10^6 eV$, designates a relativistic plasma. As the temperature of a plasma increases, the velocity discrepancies among its constituent particles also escalate. When certain particles achieve relativistic velocities, novel effects come into play, classifying these plasmas as relativistic. Typically, electrons, with their swifter disordered movements due to thermal agitation, are the particles responsible for inducing relativistic effects. Relativistic effects in plasmas within Earth's environment are generally minimal, yet there are instances where they cannot be disregarded, and this forms the focal point of the current work.

If the mean kinetic energy of electrons $< E >$ descends below the Coulomb potential V_C, representing the interaction of electrons at their mean atomic distance, plasmas adhere to non-ideal gas behavior. The boundary for this transition is illustrated by the red line in Figure (1.1), occurring when $< E >= V_C$ [5].

$$V_C = \frac{e^2}{4\pi\varepsilon_0 < r_e >} \tag{1.1}$$

In plasma classified as "degenerate," the average kinetic energy of electrons is smaller than the Fermi energy of a free electron gas. The Fermi energy represents the maximum energy state of an electron in a system at absolute zero temperature, where electrons fill the available states from the lowest energy upwards, following the Pauli exclusion principle. In degenerate plasma, the kinetic energy of electrons is constrained by this lower limit, and they tend to occupy states close to the Fermi energy, exhibiting characteristics distinct from those observed in non-degenerate plasma. This condition arises when the thermal energy of electrons is significantly smaller than the Fermi energy, resulting in unique behaviors associated with degeneracy effects [5].

$$E_F = \frac{h}{2\pi m_e}(3\pi^2 n_e)^{2/3} \tag{1.2}$$

The blue line in Fig (1.1) results from $< E >= E_F$

1.2.2 Important plasma properties

1.2.2.1 Degree of ionization

The ionization degree of a gas refers to the extent to which the gas has undergone ionization, meaning the process of converting neutral atoms or molecules into ions by removing one or more electrons. It is a measure of the proportion of atoms or molecules in a gas that have lost electrons and become positively charged ions.

The ionization degree is typically expressed as a fraction or a percentage, representing the ratio of the number of ionized particles to the total number of particles in the gas. It provides information about the level of ionization within the gas and is influenced by factors such as temperature, density, and the nature of the gas itself.

In a fully ionized gas, all or nearly all of the atoms or molecules have lost electrons, resulting in a high ionization degree. Conversely, in a weakly ionized or non-ionized gas, only a small fraction of particles may be ionized, leading to a lower ionization degree. The ionization degree is an essential parameter in plasma physics, astrophysics, and various other scientific disciplines where ionized gases play a significant role, it is defined by [6].

$$\alpha = \frac{n_i}{n_i + n_0} \tag{1.3}$$

where n_0 is the density of neutrals on m^{-3} and n_i the electron density on m^{-3} (or the

ions density).

1.2.2.2 Landau length

landau length is the distance for which the coulomb potential energy is equal to average kinetic energy (e.g the thermal energy) [6, 7]

this means

$$K_B T = \frac{ze^2}{4\pi\varepsilon_0 \lambda_L} \tag{1.4}$$

so the Landau length is given by :

$$\lambda_L = \frac{ze^2}{4\pi\varepsilon_0 K_B T} \tag{1.5}$$

for the ion charge $z = 1$ we can write

$$\lambda_L = \frac{e^2}{4\pi\varepsilon_0 K_B T} \tag{1.6}$$

The Landau length internees in the analysis of the phenomena of collisions and correlations of position in a plasma.

1.2.2.3 Debye length

Let's examine a scenario involving a positively charged particle, denoted as q, positioned at the center of a plasma. This prompts the question: Does this charged particle have an infinite range of interaction distances? The positively charged particle q exerts attractive forces on oppositely charged particles (e.g., electrons), drawing them closer, while simultaneously repelling positively charged particles (ions) with the same charge. This interaction results in the formation of an electron cloud, forming a protective shield around the particle. For this case, we can compute the potential ϕ associated with the charged particle q, representing the electric potential energy per unit charge at different distances. This calculation sheds light on the nature of the interactions and the shielding effects within the plasma.

$$E = -\nabla\phi \tag{1.7}$$

This is Gauss'low, and the poison's equation is given by

$$\nabla E = \frac{\rho(r)}{\varepsilon_0} \tag{1.8}$$

From eq (1.7) and (1.8) we can write

$$-\nabla^2\phi = \frac{\rho(r)}{\varepsilon_0} \tag{1.9}$$

Where ρ is charge density and ε_0 is permittivity of vacuum.

The particle density is given by:

$$n_e(r) = n_{0e}\exp(-\frac{-e\phi}{K_BT}) = n_{0e}\exp(\frac{e\phi}{K_BT}) \tag{1.10}$$

$$n_i(r) = Z_i n_{0i}\exp(-\frac{Z_i e\phi}{K_BT}) \tag{1.11}$$

Where n_e, n_i is electrons density and ions density , $n_{0e}, Z_i n_{0i}$ is the average value of density.

Consider the scenario where $n_0 = Z_i n_{0i} = n_{0e}$, where n_0 is constant, and we assume that electrons and ions (with charge e) have the same temperature T.

Under the condition $e\phi \ll K_BT$ (assuming that this potential is very small), these conditions enable us to expand equations (1.10) and (1.11) to the first order, resulting in the following expressions:

$$n_e(r) = n_0(1 + \frac{e\phi}{K_BT}) \tag{1.12}$$

$$n_i(r) = n_0(1 - \frac{Z_i e\phi}{K_BT}) \tag{1.13}$$

The charge density ρ is given by:

$$\rho = -e(n_e(r) - n_i(r)) + q\delta(r) \tag{1.14}$$

Here, $\delta(r)$ denotes the Dirac delta function, and q is the test charge. The first term in formula (1.14) describes polarization, and the second term represents the test charge. The formula (1.14) can be written as:

$$\rho = -en_0(\frac{e\phi}{K_BT} + \frac{Z_i e\phi}{K_BT}) + q\delta(r) \tag{1.15}$$

If we let $N_i = (Z_i + 1)$, the formula (1.15) becomes:

$$\rho = -\frac{e^2 n_0\phi}{K_BT}N_i + q\delta(r) \tag{1.16}$$

Now, using spherical coordinates for formula (1.8):

$$\nabla^2\phi = \frac{1}{r^2}\frac{d}{dr}(r^2\frac{d\phi}{dr}) = \frac{N_i e^2 n_0}{\varepsilon_0 K_BT}\phi - \frac{q}{\varepsilon_0}\delta(r) \tag{1.17}$$

We can conclude that $\frac{N_i e^2 n_0}{\varepsilon_0 K_B T}$ and $\frac{1}{r^2}$ have the same dimension. This means $\left(\frac{\varepsilon_0 K_B T}{N_i e^2 n_0}\right)^{1/2}$ is a distance.

The solution of equation (1.8) is given by:

$$\phi = \frac{q}{4\pi\varepsilon_0} \exp\left(-\frac{r}{\sqrt{\frac{\varepsilon_0 K_B T}{N_i e^2 n_0}}}\right) = \frac{q}{4\pi\varepsilon_0} \exp\left(-\frac{r}{\lambda_D}\right) \tag{1.18}$$

Where λ_D is the Debye length and is given by:

$$\lambda_D = \sqrt{\frac{\varepsilon_0 K_B T}{N_i e^2 n_0}} \tag{1.19}$$

If we assume the ions are singly-ionized, the Debye length can be expressed as:

$$\lambda_D = \sqrt{\frac{\varepsilon_0 K_B T}{e^2 n}} \tag{1.20}$$

where n is the charge density in m^{-3}.

The Debye length λ_D is a crucial parameter [7]. It was first calculated in the theory of electrolytes by Debye and Huckel in 1923 to be much smaller than the plasma size [29,30].

We can say that the Debye length represents the physical scale of the transition from plasma [31].

Figure (1.2) represents the distribution of charged particles (test particles) in plasma and vacuum [7].

The Debye radius λ_D defines a sphere known as the Debye sphere, housing N_D as the number of charges. This quantity, expressed in terms of the charge density n in m^{-3}, is given by the formula [8]:

$$N_D = n\left(\frac{4}{3}\pi\lambda_D^3\right) \tag{1.21}$$

Alternatively, for ions with charge $z = 1$, the relationship between N_D, λ_D, R_s (Wigner-Seitz radius), and λ_L (Landau length) can be established from equations (1.19), and (1.6):

$$N_D = \left(\frac{\lambda_D}{R_s}\right)^3 \tag{1.22}$$

$$N_D = \frac{\lambda_D}{3\lambda_L} \tag{1.23}$$

Here, λ_L always denotes the Landau length.

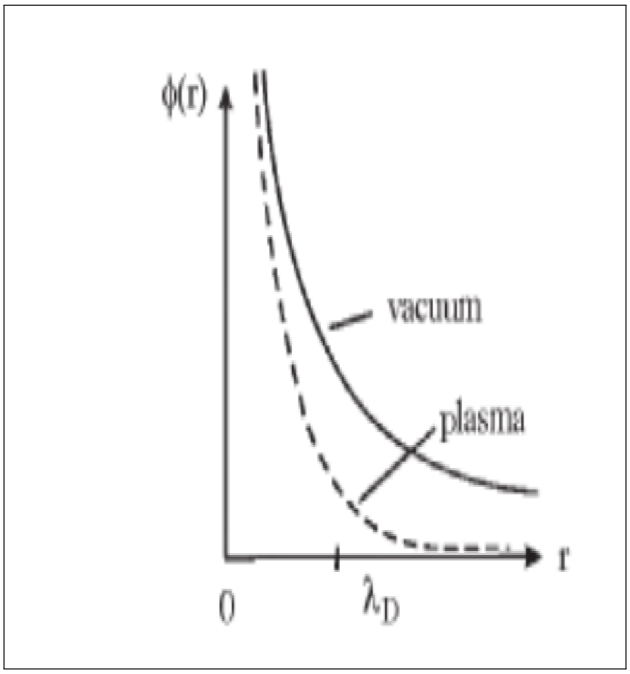

Fig 1.2: Potential distribution of a charged particle in vacuum (solid line)and in a plasma (dotted line).

We may inquire into how a plasma responds to electromagnetic waves emitted from an external source, such as particle beams [9]. This could potentially displace electrons from their equilibrium positions. The electrostatic force exerted by the ions could lead to overshooting, triggering plasma oscillations—rapid oscillations so swift that the massive ions scarcely have time to respond.

To investigate the characteristics of electron plasma oscillations, the cold plasma model is often employed. In this model, particle thermal motion and pressure gradient force are disregarded [2]. Assuming very small electron density perturbations and neglecting ion motion, we express the electron density as:

$$n_e = n_0 + n_1 \tag{1.24}$$

Here, n_0 is a constant (equilibrium electron density), n_1 represents electron density perturbation, and $n_1 \ll n_0$. The electric field $\overrightarrow{E}$ created is given by:

$$E = -\nabla\phi \tag{1.25}$$

Additionally, we have

$$\nabla^2\phi = \frac{en_1}{\varepsilon_0} \tag{1.26}$$

The equation of motion is provided by:

$$m\frac{d\overrightarrow{v}}{dt} = -e\overrightarrow{E} \tag{1.27}$$

By substituting equation (1.25) into the last formula, we derive:

$$\frac{dv}{dt} = \frac{e}{m}\nabla\phi \tag{1.28}$$

The equation of continuity is given by:

$$\frac{\partial n_e}{\partial t} + \nabla(n_e v) = 0 \tag{1.29}$$

Using equation (1.24) and considering $n_1 \ll n_0$, we arrive at:

$$\frac{\partial n_e}{\partial t} + \nabla(n_0 v) = 0 \tag{1.30}$$

This allows us to express:

$$\frac{\partial^2 n_e}{\partial t^2} + \nabla(n_0\frac{dv}{dt}) = 0 \tag{1.31}$$

Employing equations (1.28) and (1.26), we obtain:

$$\frac{\partial^2 n_e}{\partial t^2} + \frac{e^2 n_0}{m\varepsilon_0}n_e = 0 \tag{1.32}$$

Or, in written form:

$$\frac{\partial^2 n_e}{\partial t^2} + \omega_p^2 n_e = 0 \tag{1.33}$$

Here, ω_p represents the electron plasma frequency and is given by:

$$\omega_p = \left(\frac{e^2 n_0}{m\varepsilon_0}\right)^{1/2} \tag{1.34}$$

1.2.2.4 Coupling Parameter

The coupling parameter is defined as the ratio of the Coulomb energy to the thermal energy [6, 30], expressed as the Coulomb energy per particle divided by the thermal energy:

$$\Gamma = \frac{E_{\text{Coulomb}}}{K_B T} \tag{1.35}$$

The Coulomb energy per particle is given by:

$$E_{\text{Coulomb}} = \frac{q^2}{4\pi\varepsilon_0 \langle R_s \rangle} \tag{1.36}$$

Here, R_s represents the ionic radius. The coupling parameter can now be written as:

$$\Gamma = \frac{q^2}{4\pi\varepsilon_0 K_B T R_s} \sim \frac{r_L}{R_s} \tag{1.37}$$

where r_L is the Landau length. If $\Gamma \ll 1$, it implies $E_{\text{Coulomb}} \ll K_B T$, indicating low coupling. On the other hand, if $\Gamma \geqslant 1$, it implies $E_{\text{Coulomb}} \geqslant K_B T$, indicating strong coupling.

1.3 Line broadening

1.3.1 Introduction

The spectral lines emitted by plasmas are inherently non-monochromatic, displaying a certain degree of broadening attributed to the dynamic motion of particles and their collisions. Even in the absence of these factors, natural broadening persists. Spectral lines broadening is a crucial tool for investigating the plasma conditions surrounding emitted ions, providing insights into parameters such as temperature and density [3, 11].

This section delves into various mechanisms of spectral line broadening, shedding light on factors influencing line width and shape. The description of a spectral line's shape is conveniently articulated through the line profile function.

1.3.2 Profile functions

The shapes of spectral lines are described by line shape functions, denoted as I, in terms of frequency υ, angular frequency ω, or wavelength λ [1]. In this discussion, we will use angular frequency ω as it is commonly preferred.

The function I is normalized, signifying that

$$\int_{\text{line}} I(\omega)\, d\omega = 1 \tag{1.38}$$

The full width at half maximum (FWHM) in wavelength units is denoted as $\Delta\omega_{1/2}$, and the center wavelength is denoted as ω_0.

The two primary line shape functions are represented by the Gaussian and Lorentzian functions [1]. We categorize the types of line broadening in the following table:

Types	Line Broadening	Causes
Lorentzian	Natural Broadening	Result of finite radiative lifetime
Lorentzian	Collisional Broadening	Finite lifetime of quantum state due to collisions
Gaussian	Doppler Broadening	Thermal motion
Lorentzian + Gaussian	Voigt Profile	Convolution of 2-3

Table 1.1: The types of line broadening

1.3.3 Natural Broadening

In reality, the quantum states of an atom do not have a single energy but rather a small spread in energy [3]. The Heisenberg uncertainty principle connects the uncertainty ΔE of the energy E to the uncertainty in the lifetime of the state Δt, given by:

$$\Delta E \Delta t \geqslant \frac{h}{2\pi} \quad \text{or} \quad \Delta E \approx \frac{h}{2\pi\tau} \tag{1.39}$$

where h is Planck's constant and $\Delta t = \tau$ represents the lifetime.

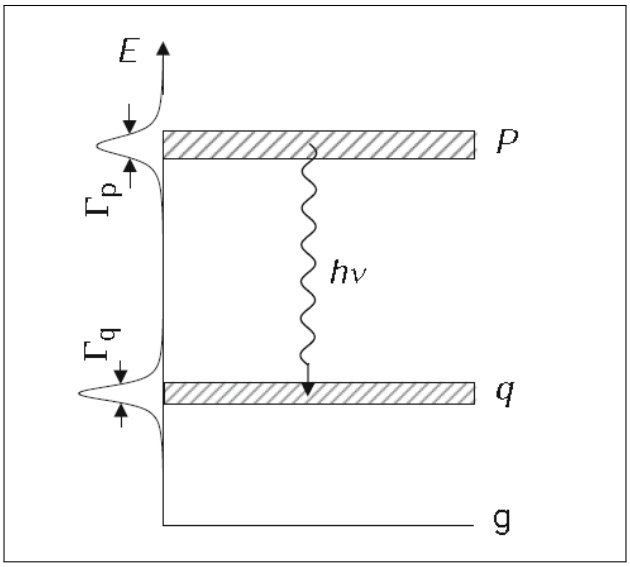

Fig 1.3: Natural width of excited energy levels [1].

A photon emitted in a transition between two energy levels (Figure 1.3 [1]) will have a range of possible frequencies:

$$\Delta\nu \approx \frac{\Delta E}{h} \approx \frac{1}{2\pi\tau} \tag{1.40}$$

The line has a Lorentzian shape and is given by [3]:

$$I(\nu) = I(\nu_0)\frac{1}{1 + \left(\frac{\nu-\nu_0}{\Delta\nu}\right)^2} \tag{1.41}$$

Here, I represents the intensity, and ν_0 is the line center. Natural broadening is always present, uniform across all wavelengths, and although usually negligible in the visible range, it can be significant for extreme ultraviolet lines of highly ionized impurities [3].

1.3.4 Doppler Broadening

Doppler broadening, associated with the Doppler effect, holds significant importance. In a plasma context, the Doppler effect is linked to disturbances caused by the movements of emitters, originating from the motion of atoms and ion emitters—the thermal velocity distribution of emitting ions. This broadening will be explored in two cases: classical and relativistic, with a detailed discussion to follow in the next chapter.

1.3.5 Collision Broadening

These effects are also variously called, such as pressure broadening, and it is also one of the most important broadening types, along with Doppler broadening [3].

Collision broadening arises from the influence of nearby particles on the emitting atom or ions [3]. There are three types of collisional broadening:

- Broadening due to collisions of the excited atom with atoms or molecules in the neutral state, known as Van Der Waals broadening.

- Broadening due to collisions of the excited atom with atoms or molecules of the same nature, leading to a resonant transition, called resonance.

- Stark broadening, which arises from the collision of charged particles (electrons and ions) and is usually dominant in plasma. The central mechanism for Stark broadening is the electrostatic field generated by the perturber on the radiator [1].

Detailed calculations of Stark broadening are extremely complicated; see Griem (1964) or Breene 1961 [32].

1.3.6 Broadening due to Magnetic Field Effects

In 1896, Zeeman discovered that the lines of series spectra could be influenced by magnetic fields, a phenomenon now known as the Zeeman effect [33].

The interaction of a magnetic field with the kinetic moment of the atom causes a disturbance, leading to the lifting of degeneracy in energy levels. This disturbance is reflected in the observed profile [1].

For more details, refer to [32–35].

1.3.6.1 Combinations of Broadening Effects

In some cases, both Doppler and magnetic field effects may be present. If there are two independent profiles, denoted as $I_1(\Delta\nu)$ and $I_2(\Delta\nu)$, the convolution of these two profile functions is given by [3]:

$$I(\Delta\nu) = \int I_1(\Delta\nu - \Delta\nu')I_2(\Delta\nu')d(\Delta\nu') \tag{1.42}$$

1.4 Conclusion

In conclusion, this chapter has laid the groundwork for understanding the complexities of spectral line broadening in plasmas. Starting with an introduction to plasma physics and its foundational properties, we explored the classification of plasmas based on temperature and electron density. The subsequent sections delved into essential plasma properties such as the degree of ionization, Landau length, and Debye length.

The coupling parameter was introduced as a measure of the ratio between Coulomb energy and thermal energy, offering insights into the degree of coupling within the plasma. We then transitioned into the realm of line broadening, emphasizing its crucial role in unraveling plasma conditions.

Natural broadening, arising from the uncertainty principle and finite radiative lifetime, sets the stage for spectral line shapes. Doppler broadening, driven by thermal motion, and collisional broadening, influenced by interactions with nearby particles, were explored in detail. Additionally, the effects of magnetic fields on spectral lines, known as the Zeeman effect, were introduced.

The chapter concluded by addressing the combinations of broadening effects, especially the convolution of Doppler and magnetic field effects. These insights pave the way for a deeper understanding of the diverse factors influencing the width and shape of spectral lines emitted by plasmas.

In the subsequent chapters, we will delve into specific cases of Doppler and magnetic field effects, providing detailed calculations and analyses. The knowledge gained from this foundational chapter will serve as a cornerstone for unraveling the intricacies of plasma physics and its diagnostic potential through spectral line studies.

Chapter 2

The Relativistic and Non-relativistic Doppler Broadening

2.1 Introduction

The Doppler effect, also known as the Doppler shift, stands as one of the most universally recognized phenomena in physics, manifesting in both light and sound. Originating from Christian Johann Doppler's discovery in 1842, where he posited its applicability to both sound and light, the effect hinges on an object's relative motion determining whether its emitted light increases or decreases. Given its paramount significance, this effect undergoes thorough examination across the global scientific community.

The Doppler effect has found rich utility in various scientific realms, permeating technology and science alike [20, 24, 36–38]. Applications span diverse fields such as medicine, where Doppler-shifted ultrasonic waves screen blood flow in veins, to determining lifetimes of excited atomic states [39]. In astronomy, it plays a pivotal role, aiding in the calculation of speed, direction, and rotational dynamics of stars and galaxies, even contributing to the discovery of dark matter [22].

Within a plasma environment, atoms or ions emitting radiation can be likened to signal sources, each moving with speeds adhering to the law of speed distribution. The resultant radiation experiences the Doppler effect, specifically Doppler broadening, a collective phenomenon explored extensively in plasma spectroscopy through various research endeavors.

In ultra-hot plasmas, where emitters move at velocities significantly surpassing the speed of light, relativity becomes a crucial consideration. This scenario occurs in laser implosion, astrophysics, and high-temperature laser technology. The Doppler effect dominates in such conditions, particularly when temperatures range from 10^8 to 10^{12} K and

densities remain below 10^{24} cm^{-3}.

This chapter delves into classical Doppler broadening, grounded in the non-relativistic Doppler effect and Maxwell speed distribution. The classical Doppler broadening is presented as a standard formula. Additionally, the chapter explores the relativistic Doppler effect, offering a novel formula for the intensity of line shapes in relativistic Doppler broadening : a departure from existing methods. A new Full Width at Half Maximum (FWHM) formula for the corresponding profile, distinct from its non-relativistic counterpart, is also introduced.

2.2 The Non-relativistic Doppler Broadening

2.2.1 The classical Doppler effect

In school, students are taught the classical example of the Doppler effect using a moving ambulance sounding its whistle toward a stationary observer. The observer detects a change in the ambulance whistle.

The Doppler effect is defined as a crucial phenomenon that correlates the frequency of harmonic waves generated by a moving source with the frequency measured by an observer moving at a different velocity from that of the source [40].

In plasma, radiation emission (or absorption) by a particle (atom, ion, etc.) often occurs during movement. The Doppler effect causes the observed frequency in the observer's frame (at rest) to differ from the frequency emitted in the atom's frame. The mean particle velocity at thermodynamic equilibrium is linked to the medium's temperature, connecting the broadening of the statistical Doppler effect to the distribution of emitter velocities at temperature T and emitter mass m.

Consider a motionless observer viewing an emitting atom moving with velocity V at an angle θ with the observation direction Ox (Fig 2.1).

At the moment t_0, the emitter emits a luminous signal, received by the observer at position O at moment t_1 given by:

$$t_1 = \frac{D}{c} \tag{2.1}$$

Where D is the distance between the emitter and observer at moment t_0, and c is the velocity of light in a vacuum. At moment t_2, where $T_0 = \Delta t_0 = t_2 - t_0$, the emitter emits a second luminous signal received by the observer at position O at t_3 given by:

$$t_3 = T_0 + \frac{D + d}{c} \tag{2.2}$$

Where $d = V_x T_0$ is the distance traveled by the emitter. If the emitter moves toward

the observer, the distance is written as $D - d$, so

$$t_3 = T_0 + \frac{D + V_x T_0}{c} \tag{2.3}$$

The period T with respect to the periodontal is given by:

$$T = \Delta t = t_3 - t_1 = T_0 + \frac{D + V_x T_0}{c} - \frac{D}{c} \tag{2.4}$$

$$= T_0 \left(1 + \frac{V_x}{c}\right) = T_0 \left(1 + \frac{V \cos\theta}{c}\right) \tag{2.5}$$

Consequently, the angular frequency is given by:

$$\omega(V_x) = \omega_0 \left(1 - \frac{V \cos\theta}{c}\right) = \omega_0 \left(1 - \frac{V_x}{c}\right) \tag{2.6}$$

where ω is the angular frequency, and ω_0 is the angular eigenfrequency.

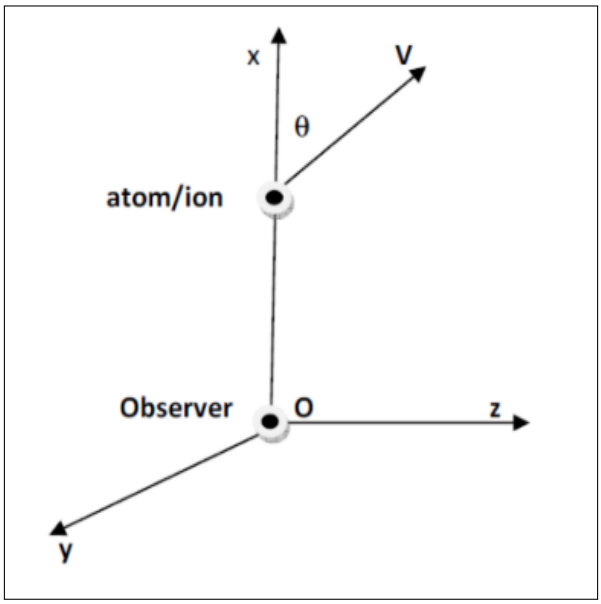

Fig 2.1: The fixed frame where the emitter moves with a velocity V forming an angle θ with the observation direction Ox.

2.2.2 The Classical Doppler Broadening (Non-relativistic Case)

As discussed in Chapter One, spectral line broadening plays a crucial role in spectroscopic diagnostics of various laboratory and astrophysical plasmas. Doppler broadening, attributed to the movement of emitting ions, is a distinctive mechanism where the fre-

quency of the detected photon in the laboratory frame, denoted as ω, differs from the frequency emitted in the frame of the moving ion, denoted as ω_0.

The relation between angular frequencies ω and ω_0 is given by Eq (2.6). The line's normalized intensity (normalized to one) at the angular frequency ω is determined by averaging over the normalized Maxwell distribution, denoted as $f_{Maxwell}(V_x)$, which is given by:

$$f_{Maxwell}(V_x) = \left(\frac{m}{2\pi K_B T}\right)^{1/2} \exp\left(-\frac{mV_x^2}{2K_B T}\right) \tag{2.7}$$

The Dirac delta distribution is then applied:

$$I(\omega) = \langle \delta(\omega - \omega(V_x)) \rangle_{Maxwell} = \sqrt{\frac{m}{2\pi K_B T}} \int_{-\infty}^{+\infty} \exp\left(-\frac{m}{2K_B T} V_x^2\right) \delta(\omega - \omega(V_x)) dV_x \tag{2.8}$$

Utilizing the integral representation of the Dirac delta distribution, where u is the integration variable with units of seconds:

$$\delta(\omega - \omega(V_x)) = \frac{1}{2\pi} \int_{-\infty}^{+\infty} \exp\left(iu(\omega - \omega(V_x))\right) du \tag{2.9}$$

The normalized intensity (normalized to one) is obtained:

$$\begin{aligned} I(\omega) = \frac{1}{2\pi}\sqrt{\frac{m}{2\pi K_B T}} \int_{-\infty}^{+\infty} \exp(iu\omega) du \\ \times \int_{-\infty}^{+\infty} \exp\left(-\frac{m}{2K_B T} V_x^2 - iu\omega(V_x)\right) dV_x \end{aligned} \tag{2.10}$$

Simplifying, we get:

$$I(\omega) = \frac{1}{2\pi}\sqrt{\frac{2\pi mc^2}{K_B T \omega_0^2}} \exp\left(-\frac{mc^2}{2K_B T}(\varpi - 1)^2\right) \tag{2.11}$$

Here, $\varpi = \frac{\omega}{\omega_0}$, K_B is the Boltzmann constant, and m is the emitter mass. This formula represents the intensity of the line in the non-relativistic case. It is symmetric (Gaussian) around the central angular frequency ω_0. Note that the integrals in formula (2.11) are strongly convergent due to dealing with purely Gaussian integrals.

The Full Width at Half Maximum (FWHM) is given by the well-known formula (in angular frequency units):

$$\Delta\omega_{Doppler} = \omega_0 \sqrt{\frac{8K_B T \ln(2)}{mc^2}} = 7.1574 \times 10^{-7} \omega_0 \sqrt{\frac{T}{M}} \tag{2.12}$$

Here, M is the mass of the emitter in atomic mass units, T is the temperature in Kelvin, and the relationship between temperature and FWHM in the classical case is evident in formula (2.12).

2.3 The relativistic Doppler Broadening

2.3.1 The relativistic Doppler effect

2.3.1.1 Introduction

In ultra-hot plasma, the emitters of radiation move at extremely high velocities in comparison to the speed of light. We encounter this type of plasma in the case of laser implosion, astrophysics, and laser technology at very high temperatures. So, it is necessary to consider the relativity of the emitter's movement. In this case where the temperature ranges from 10^8 to $10^{12}K$, and the density $\leq 10^{24}cm^{-3}$, the Doppler effect is dominant.

2.3.2 Lorentz Transformations

The goal of relativity is to explain and understand how motion looks from different perspectives, particularly from different moving frames.

Lorentz transformation is the mathematical relationship between two coordinate frames that move at a constant velocity relative to each other. Named after Dutch physicist Hendrik Lorentz, this transformation is a type of linear transformation, preserving operations such as scalar multiplication and addition within vector spaces. In the context of special relativity, Lorentz transformations are specifically concerned with changes in inertial frames.

To perform this transformation, an observer moving at different speeds can measure different times, distances, and events chronologically. The crucial requirement is that the speed of light must remain constant in all inertial frames.

Lorentz Transformation Equations

Assuming that frame F is a stationary reference frame, with coordinates x, y, z, and t defined, consider another reference frame F', moving at a velocity v relative to F. The observer defines coordinates x', y', z', and t', which are perpendicular in both frames. In this scenario, the relative motion occurs along the x'-axis, meaning both reference frames share the same origins at $(0, 0, 0)$.

These coordinates, when recorded in reference frame F', can be expressed as [41, 42]:

$$t' = \gamma\left(t - \frac{Vx}{c^2}\right) \tag{2.13}$$

$$x' = \gamma\left(x - Vt\right) \tag{2.14}$$

$$y' = y \tag{2.15}$$

$$z' = z \tag{2.16}$$

Here, $\gamma = \sqrt{\frac{1}{1-\frac{V^2}{c^2}}}$.

2.3.2.1 The Relativistic Doppler Effect

The relativistic Doppler effect is one of the most significant applications of Lorentz transformations.

We assume the emitter in Figure 2.1 has a relativistic velocity. For a more sophisticated analysis involving Lorentz transformations, we must use them. Taking the first Lorentz transformation and using it in Formula (2.4), we find that since the emitter is moving with respect to the observer's frame, the time taken to release a single wavelength is given by:

$$\Delta t' = \gamma \Delta t \tag{2.17}$$

where $x = 0$.

Formula (2.4) becomes:

$$T = \gamma T_0 + \frac{\gamma V_x}{c} T_0 \tag{2.18}$$

$$T = \gamma(1 + \frac{V_x}{c})T_0 \tag{2.19}$$

where $\gamma = \sqrt{\frac{1}{1-\frac{V^2}{c^2}}}$.

Now we can write Formula (2.6) in the relativistic case as [42]:

$$\omega(\beta) = \omega_0 \gamma(1 - \beta\cos\theta) \tag{2.20}$$

where $\beta = \frac{V}{c}$, $\gamma = \frac{1}{\sqrt{1-\beta^2}}$, ω_0 is the angular eigenfrequency, and θ is the angle between the velocity of the emitter and the observation direction (OX) (Figure 2.1).

2.3.3 The Relativistic Doppler Broadening

In the relativistic case, using the normalized Juttner-Maxwell distribution (normalized to one) [43]:

$$W_{J-M}(\beta)d\beta = \lambda \frac{\gamma^5\beta^2}{K_2[\lambda]} \exp(-\lambda\gamma)d\beta \tag{2.21}$$

where

$$\lambda = \frac{mc^2}{K_B T} \tag{2.22}$$

and $K_2[X]$ is the modified Bessel function of order two, we obtain the normalized relativistic intensity (normalized to one) of the line profile:

$$\begin{aligned} I(\omega) &= < \delta(\omega - \omega(\beta)) >_{Juttner-Maxwell} \\ &= \frac{1}{2\pi}\int_{-\infty}^{+\infty} du \int\int\int W_{J-M}(\beta)d\beta \exp(iu(\omega - \omega(\beta)))du \sin\theta d\theta d\phi \end{aligned} \tag{2.23}$$

Here, we have introduced the integral over the spherical angles that makes the emitter velocity with the fixed frame axis (see Figure 2.1). We have replaced the Dirac delta distribution by its integral representation by integrating over the variable u. Replacing the Juttner-Maxwell distribution $W_{J-M}(\beta)$ given by Formula (2.21) and $\omega(\beta)$ given by Formula (2.20), we reach a more suitable expression for the relativistic intensity of the line profile:

$$I(\omega) = \frac{\lambda}{2K_2[\lambda]} \int_1^{\infty} \gamma d\gamma \exp(-\lambda\gamma) \left(\text{sign}(\varpi - \gamma + \sqrt{\gamma^2 - 1}) - \text{sign}(\varpi - \gamma - \sqrt{\gamma^2 - 1})\right) \tag{2.24}$$

where $\text{sign}(t) = +1$ if $t \succ 0$ and $\text{sign}(t) = -1$ if $t \prec -1$, and $\varpi = \frac{\omega}{\omega_0}$ is the reduced angular frequency. We can simplify the formula for numerical treatment:

$$\begin{aligned} I(\omega) = \frac{\lambda}{2K_2[\lambda]} \exp(-\lambda) \int_1^{\infty} \gamma d\gamma \exp(-\lambda(\gamma - 1)) \\ \times \left(\text{sign}(\varpi - \gamma + \sqrt{\gamma^2 - 1}) - \text{sign}(\varpi - \gamma - \sqrt{\gamma^2 - 1})\right) \end{aligned} \tag{2.25}$$

If we put $\lambda(\gamma - 1) = y$, according to [44]:

$$I(\omega) = \frac{\exp(-\lambda)}{2K_2[\lambda]} \int_0^\infty (\frac{y}{\lambda} + 1) dy \exp(-y) \tag{2.26}$$
$$\times \left(S(\varpi - \frac{y}{\lambda} - 1 + \sqrt{\left(\frac{y}{\lambda}\right)^2 + 2\frac{y}{\lambda}}) \quad - S(\varpi - \frac{y}{\lambda} - 1 - \sqrt{\left(\frac{y}{\lambda}\right)^2 + 2\frac{y}{\lambda}}) \right)$$

We note that the integral in the last formula is convergent because we deal with the integral in the distribution sense [45].

To find the Full Width at Half Maximum (FWHM) for the relativistic case, we can write the last formula as:

$$\frac{2K_2[\lambda]}{\lambda} I(\varpi) = \int_1^\infty \gamma d\gamma \exp(-\lambda\gamma) \left(\text{sign}(\varpi - \gamma + \sqrt{\gamma^2 - 1}) - \text{sign}(\varpi - \gamma - \sqrt{\gamma^2 - 1}) \right) \tag{2.27}$$

After integrating over λ on both sides, we get:

$$I(\varpi) \int \frac{2K_2[\lambda]}{\lambda} d\lambda = - \int_1^\infty d\gamma \exp(-\lambda\gamma) \left(\text{sign}(\varpi - \gamma + \sqrt{\gamma^2 - 1}) - \text{sign}(\varpi - \gamma - \sqrt{\gamma^2 - 1}) \right) \tag{2.28}$$

The right side integration (integration by parts) gives:

$$\begin{aligned} I(\varpi) \int \frac{2K_2[\lambda]}{\lambda} d\lambda = & - \frac{2}{\lambda} \int_1^\infty d\gamma \exp(-\lambda\gamma) \\ & \times \left[\left(-1 + \frac{\gamma}{\sqrt{\gamma^2 - 1}} \right) \delta \left(\varpi - \gamma + \sqrt{\gamma^2 - 1} \right) \right. \\ & \left. + \left(1 + \frac{\gamma}{\sqrt{\gamma^2 - 1}} \right) \delta \left(\varpi - \gamma - \sqrt{\gamma^2 - 1} \right) \right] \end{aligned} \tag{2.29}$$

Where $\delta(x)$ is the Dirac delta function.

Both occurrences of $\delta(x)$ in the last expression hold at $\gamma_0 = \frac{\varpi^2+1}{2\varpi}$. Using the properties of $\delta'(f(x)) = \frac{\delta(x-x_0)}{|f'(x_0)|}$, the formula (2.30) transforms as:

$$\begin{aligned} I(\varpi) \int \frac{2K_2[\lambda]}{\lambda} d\lambda = & -\frac{2}{\lambda} \int_1^{+\infty} d\lambda \exp(-\lambda\gamma) \\ & \times \left[(-1 + \gamma\Gamma) \frac{\delta(\varpi - \gamma_0)}{(-1 + \gamma_0\Gamma_0)} + (1 + \gamma\Gamma) \frac{\delta(\varpi - \gamma_0)}{(1 + \gamma_0\Gamma_0)} \right] \end{aligned} \tag{2.30}$$

Where $\Gamma = \frac{1}{\sqrt{\gamma^2-1}}$, and after using $\delta(x)$ properties we can write:

$$I(\varpi)\int \frac{2K_2[\lambda]}{\lambda}d\lambda = -\frac{4}{\lambda}\exp(-\lambda\gamma_0) \tag{2.31}$$

Now, making the derivative on both sides of the last formula with respect to λ, we find immediately:

$$I(\varpi) = \frac{2}{K_2[\lambda]}\left(\frac{1}{\lambda}+\frac{\varpi^2+1}{2\varpi}\right)\exp\left(-\lambda\frac{\varpi^2+1}{2\varpi}\right) \tag{2.32}$$

The corrected text is as follows:

"The last formula is simplified from formula (2.24), and this formula gives the relativistic Doppler profile. It is evident that the profile in formula (2.32) is not Gaussian and not symmetric, whereas the non-relativistic Doppler profile (2.11) is. It is also easy to verify that formula (2.32) approaches the non-relativistic formula (2.11) up to a factor (frequency independent) when c goes to infinity.

Another feature of the relativistic Doppler profile is that the maximum of the intensity is reached, as in the case of the non-relativistic Doppler profile, when ω is equal to the unperturbed frequency ω_0. This result is not surprising because the ions (emitters of the radiation) are in random motion, and statistically, there are as many ions moving towards the observer as there are fleeing from the observer. Furthermore, both the relativistic Doppler profile and the non-relativistic Doppler profile are not particle density dependent. Concerning the asymmetry of the relativistic profile, it will be the subject of the study presented in the next chapter.

It is easy now to compute the Full Width at Half Maximum (FWHM) of the new profile (2.32). A simple algebraic operation gives the new FWHM for the relativistic Doppler profile, where it is given by:

$$\Delta\varpi_{RD} = 2\sqrt{\left(\frac{\Lambda_0(\lambda)}{\lambda}\right)^2 - 1}$$

And we have

$$\Delta\omega_{RD} = \omega_0\Delta\varpi_{RD} = 2\omega_0\sqrt{\left(\frac{\Lambda_0(\lambda)}{\lambda}\right)^2 + 1} \tag{2.33}$$

Such that Λ_0 is the solution of the transcendental equation:

$$\exp(-\Lambda) = \frac{1}{2}\left(\frac{1+\lambda}{1+\Lambda}\right)\exp(-\lambda) \tag{2.34}$$

Following formula (2.12) and formula (2.33), the ratio between the relativistic Doppler

broadening and the non-relativistic Doppler broadening is then given by:

$$\text{ratio} = \frac{\Delta\omega_{RD}}{\Delta\omega_{NRD}} = \sqrt{\frac{\Lambda_0^2}{2\lambda \log 2}} \tag{2.35}$$

The relativistic Doppler profile, described by formula (2.32), reveals intriguing characteristics that distinguish it from its non-relativistic counterpart (2.11). The absence of Gaussian symmetry in the relativistic profile is a significant departure from the non-relativistic case, highlighting the impact of relativistic effects on the line shape. This lack of symmetry implies that the probability distribution of frequencies is not centered around the unperturbed frequency, and there is a noticeable skewness in the distribution.

The fact that the maximum intensity is attained when ω is equal to the unperturbed frequency ω_0 echoes a similar behavior observed in the non-relativistic Doppler profile. This outcome is intuitively understandable as, in a system with randomly moving ions, the statistical balance between ions moving towards and away from the observer results in a peak intensity at the unperturbed frequency. This symmetry in the distribution of ions contributes to the consistency in the location of the intensity maxima in both relativistic and non-relativistic scenarios.

Moreover, it is noteworthy that the relativistic Doppler profile, like its non-relativistic counterpart, does not depend on particle density. This independence from particle density implies that the observed line shape is not significantly influenced by the number of emitters, indicating a certain level of universality in the relativistic Doppler broadening process.

The asymmetry present in the relativistic Doppler profile opens avenues for further investigation, as mentioned in the text. Understanding the sources and implications of this asymmetry could provide valuable insights into the underlying physical processes and aid in the interpretation of observed spectral lines in astrophysical and laboratory settings.

Moving on to the calculation of the Full Width at Half Maximum (FWHM) of the relativistic Doppler profile, expressed in formula (2.33), introduces a quantitative measure of the line width. The FWHM characterizes the extent of the spectral line at half of its maximum intensity, offering a valuable metric for comparing line shapes and assessing the impact of relativistic effects. The transcendental equation involving Λ_0 underscores the complexity of determining the broadening parameter in the relativistic context.

The ratio defined in formula (2.35) provides a succinct measure of how the relativistic Doppler broadening compares to its non-relativistic counterpart. The square root of $\frac{\Lambda_0^2}{2\lambda \log 2}$ encapsulates the relative increase in broadening due to relativistic effects with

increasing temperature. This dimensionless ratio serves as a universal factor applicable across different transitions, emphasizing the generic nature of the relativistic Doppler broadening enhancement.

2.4 Conclusion

In this chapter, we explored classical Doppler broadening in the non-relativistic context, characterized by the familiar Gaussian profile associated with the utilization of a Maxwell distribution for emitter velocities. The classical Full Width at Half Maximum (FWHM) formula for the Gaussian profile was also derived. To extend our analysis to relativistic scenarios, accounting for the potential high velocities of emitters, we introduced a novel expression for relativistic Doppler broadening. This formulation necessitates considering an appropriate velocity distribution for emitters. Notably, our findings revealed an asymmetry in the Doppler broadening, a departure from the symmetric nature of the well-known classical Gaussian. Moreover, we derived a distinct FWHM formula specific to the relativistic case, highlighting the nuanced features introduced by relativistic effects on spectral line shapes. This exploration provides valuable insights into the complex interplay between velocity distributions and broadening mechanisms, enhancing our understanding of Doppler broadening phenomena across classical and relativistic regimes.

Chapter 3

Results and Discussion

3.1 Introduction

Natural line broadening, Instrumental broadening, Doppler broadening, Electron impact broadening, and Quasi-static Stark broadening, all these spectral line-broadening effects contribute to the total line width as a combination of these factors. Typically, one of these effects dominantly influences the line width, depending on the local plasma temperature and density, while the others are considered smaller corrections to the dominating one [11].

For instance, in [46], the Doppler broadening of the Xe^{+44} $3C$ transition with energy $E = 4858eV$ was examined. In an equilibrium plasma where the ion temperature equaled the electron temperature at 2 keV, the Doppler broadening constituted 35.9% of the total width, while the Stark broadening was 51.28%.

In many laboratory plasmas, Doppler broadening tends to be dominant, especially in high-temperature plasmas of moderate density, such as those found in magnetic fusion [3]. Another example pertains to the relativistic electronic broadening of the ly-α line of Hydrogen-like silver (Ag^{+46}) with the Juttner-Maxwell distribution, observed in a high-temperature and high-density environment with $T = 8.3 \times 10^9 K$ and $Ne = 10^{24}\ cm^{-3}$ see ref [17], where, in this temperature range, the Doppler effect dominates.

Within this chapter, we embark on an in-depth exploration, conducting a meticulous comparative analysis between the effects of relativistic and non-relativistic Doppler broadening on spectral line profiles specifically within ultra-hot plasmas. The scope of our investigation extends to the study of broadening induced by the Doppler effect across a diverse array of ions, including Helium-like and Hydrogen-like Chrome, helium-like and Hydrogen-like Iron, Hydrogen-like Vanadium, and Copernicium.

A crucial facet of our examination within this chapter involves a detailed comparison between Doppler and Stark widths in both classical and relativistic scenarios, specifically

focusing on $Ly-\alpha$ lines emitted by hydrogen-like ions. This comparison serves to shed light on the distinct characteristics of these two broadening mechanisms under different physical conditions. Notably, we integrate experimental results into this comparative analysis, providing a holistic perspective that combines theoretical predictions with empirical observations.

3.2 Comparison of the impacts of relativistic and non-relativistic Doppler broadening.

To ensure the validity and reliability of our investigation, we have rigorously conducted comparisons between our theoretical predictions and experimental results, which are presented comprehensively in this chapter. However, it is crucial to underscore a significant caveat before delving into these comparisons. Despite the current lack of experimental evidence confirming the production of Cn^{+111} at 100 KeV ($T = 10^9 K$), this absence does not preclude the theoretical exploration of its emission profile. Our theoretical framework extends its applicability even to temperatures slightly exceeding this threshold.

Adding further context to our study, we highlight that the longest-lived confirmed isotope, 285 Cn, possesses a half-life of 29 seconds. This temporal constraint frames our investigation within a realistic context. To bolster our arguments, we present Table 3.1, offering a detailed breakdown of the percentage representation of Cn^{+111} across various β values ($\beta = v/c$). This tabular representation contributes valuable insights into the prevalence of Cn^{+111} under distinct velocity regimes, enhancing the depth of our study.

$\beta \times 10^{-4}$	2	4	6	8	10	12	16	20
percent	98	91	77	57.5	37.5	21.5	4.71	0.6

Table 3.1: Comparison between the percentages of relativistic ions for different values of β

The information gleaned from the table is quite revealing. The data clearly illustrates that only a minute fraction, precisely 0.6 percent, of Cn^{+111} ions exhibit velocities exceeding $\beta > 0.002$ at a temperature of $10^9 K$. This finding signifies the presence of trace amounts of high-velocity Cn^{+111} ions in the given plasma conditions. The majority of Cn^{+111} ions, accounting for 99.4 percent, have velocities below this threshold. The velocities of these ions, as indicated by the value of β, play a significant role in understanding their behavior within the plasma. The rarity of Cn^{+111} ions with velocities above 0.002 implies that the distribution of velocities within this ion species is skewed towards lower values in the specified high-temperature environment. This nuanced insight into the ve-

locity distribution becomes pivotal for comprehending the dynamic characteristics and behavior of Cn^{+111} ions under such extreme thermal conditions.

3.2.1 Asymmetric broadening

So unlike the classical Doppler effect, the relativistic one has a property an asymmetric broadening corresponding to the temperatures in the range (10^5–10^9 K). We remark also that in the relativistic case, as in the classical case, the central frequency is unchanged. The maximum value of the intensity is at omega underbar= 1 both for the classical and relativistic case as we see in the figure (3.1) for Iron and figure (3.2) for Coperniciom. This result is expected since the ions (emitters of the radiation) exhibit random motion, with an equal statistical distribution of ions moving towards and away from the observer.

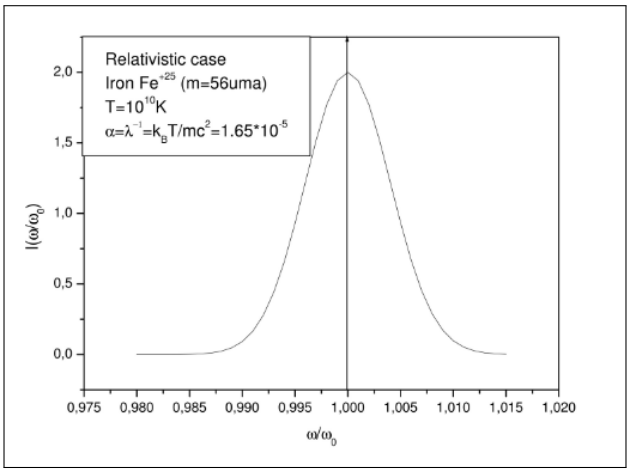

Fig 3.1: Relativistic intensity as defined by Formula 2.25 for Iron at Fe^{+25} at T = 1.9 10^9 K

If we characterize the asymmetry using the formula provided below :

$$Asym = I(\omega, relativistic) - I(\omega, classical) \tag{3.1}$$

The asymmetry, as formulated in formula 3.1, signifies the disparity between relativistic and classical intensities. The determination of asymmetry, as per [47], involves calculating the difference between the normalized relativistic intensity (expressed by Equation 2.25) and the normalized classical intensity (articulated in Equation 2.11). This process yields the asymmetry profile for Cn^{+111} at a temperature of 1.9×10^9 K. Through this analysis, we gain a nuanced understanding of the intricate interplay between relativistic and classical intensity profiles, providing valuable insights into the distinctive asymmetry features observed in spectral lines.

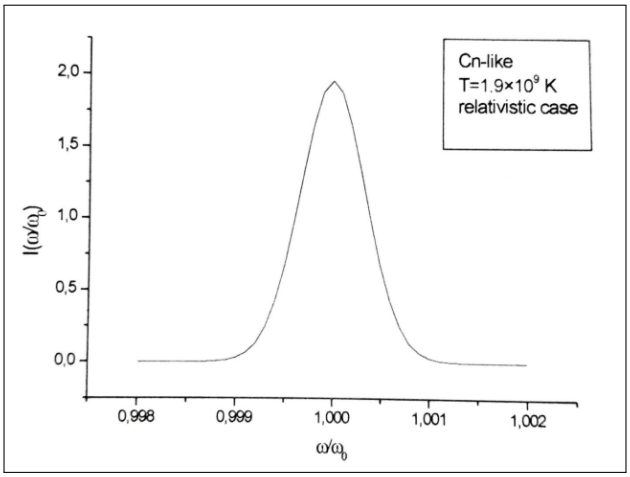

Fig 3.2: Relativistic intensity as defined by Formula 2.25 for for Cn^{+111}

In Figure 3.3, we see clearly that, in the left of $\varpi = \omega/\omega_0 = 1.00007$, the intensity of the relativistic profile is lower than of the classical profile, whereas it is higher in the right of $\varpi = \omega/\omega_0 = 1.00007$. It can be seen clearly in this figure that the asymmetry is a function of $(\varpi = \omega/\omega_0)$ and that means that for any line, the asymmetry is as indicated in this figure. To obtain the asymmetry, for a specific line centered at ω_0, we must multiply ϖ by ω_0. The same remark holds for Figure 3.4 for the hydrogen-like Iron.

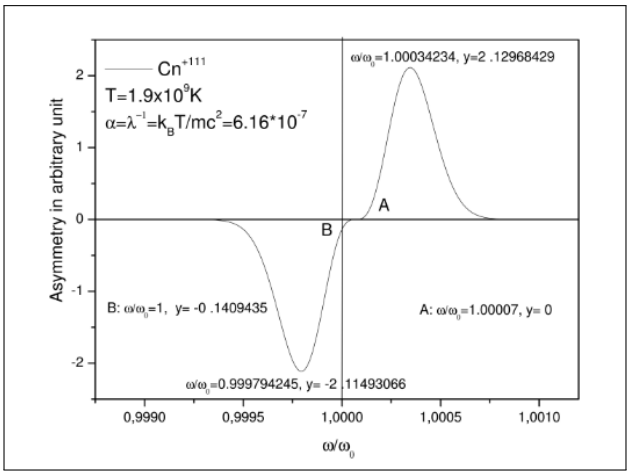

Fig 3.3: Relativistic intensity as defined by Formula 3.1 for for Cn^{+111}

However, there is a more notable imbalance, given that the maximum asymmetry reaches 2.40 for iron (Fe^{+25}), whereas it is 2.12 for Copernicus (Cn^{+111}). Another aspect to consider is that the line profile remains unspecified due to the utilization of the reduced angular frequency $\varpi = \frac{\omega}{\omega_0}$. To delineate the intensity $I(\omega)$ for each specific transition, one must multiply ϖ (the x-axis) by the corresponding angular eigenfrequency ω_0. This

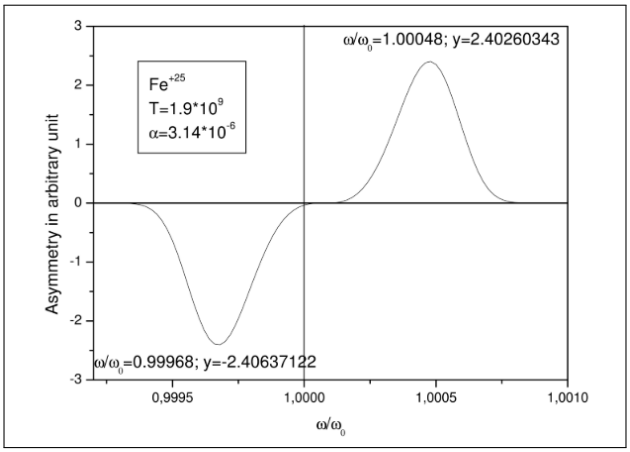

Fig 3.4: Relativistic intensity as defined by Formula 3.1 for Iron at Fe^{+25} at T = $1.9.10^9$ K

asymmetry is also evident in Figure (3.5), which illustrates the line profile of the Vanadium ion (Vn^{+22}).

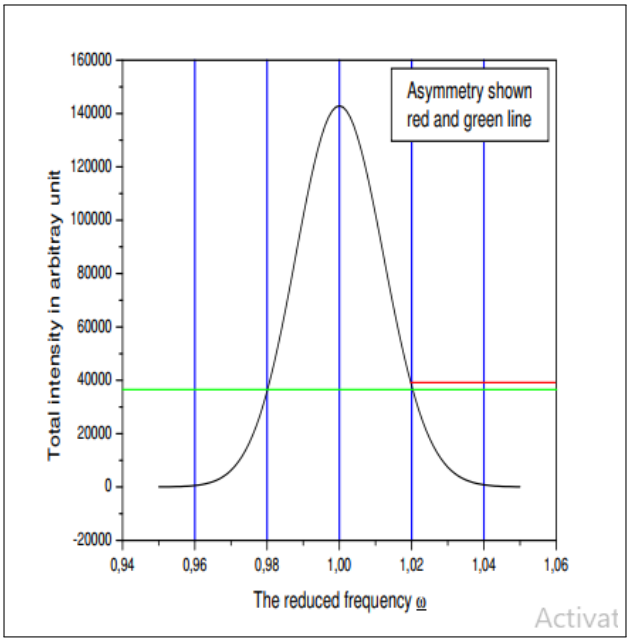

Fig 3.5: line of transition $n = 6$ to $n = 5$ Vn^{+22} with shown asymmetry (Collision and Doppler Broadening are included) for $T = 8.02 \times 10^{10} K$, $Ne = 1020 cm^{-3}$ for $Z = 23$

In Table 3.2, we denote by $\omega_{L,R}$ the values of the reduced angular frequency at the left and right sides of the peak of the $Ly - \alpha$ line (centered at $\omega = \omega_0 = 127948.800\,\text{eV}$) of Cn^{+111} (synthesized in laboratories for use in nuclear reactions [44]).

ω_L and ω_R are chosen to be symmetrical with respect to the center of the line at $\omega = \omega_0$, resulting in intensities very close to half of the maximum intensity.

As shown in Table 3.2, which presents Asymmetry percentages $A(\%)$ for different temperatures for $Ly-\alpha$ of Cn^{+111}, with $\omega_0 = 127948.800\,\text{eV}$, $I_L = I(\omega_L) \times 10^4$, and $I_R = I(\omega_R) \times 10^4$ the intensity value at the right, $I(\omega_R)$, is greater than the intensity at the left, $I(\omega_L)$. This observation clearly indicates that the line profile exhibits asymmetry as defined by [48].

$T(K)$	10^9	4×10^9	8×10^9	10^{10}
ω_L	127689.8	127663.8	127546.8	127498.8
ω_R	128206.8	128233.8	127349.8	128398.8
I_L	3.32427	8.23569	5 : 84469	5.20331
I_R	3.3836	8.2759	5.86482	5.21939
$A(\%)$	0.884	0.273	0.172	0.15

Table 3.2: Asymmetry percentages $A(\%)$ for different temperatures for $Ly-\alpha$ of Cn^{+111}.

To illustrate symmetry, we depicted the relativistic Doppler broadening of $Ly-\alpha$ line across various elements and temperatures. See Figures (3.9, 3.10, and 3.11)for details.

3.2.2 Comparison of Theories

In Table 3.3, we have computed the Full Width at Half Maximum (FWHM) of ly-α ($1s^2$-1s2p) [49] for various hydrogen-like ions under both relativistic and classical conditions. Upon examination of Table 3.3, it becomes evident that the FWHM values differ slightly between the relativistic and classical cases. Moreover, the ratio $\frac{\text{FWHM}_r}{\text{FWHM}_c}$ increases with temperature.

H-like ions	W^{+73}	Fe^{+25}	Fe^{+25}	Fm^{+99}	Cn^{+111}
T(K)	8.5×10^8	1.9×10^9	10^{10}	1.5×10^9	1.9×10^9
$\text{FWHM}_{classical}$ (eV)	92.474594	29.00004	66.5306	206.5869	236.4535
$\text{FWHM}_{relativistic}$ (eV)	92,26113	29.00754	66.54833	206,64004	236.51435
$\frac{\text{FWHM}_r}{\text{FWHM}_c}$	0,99769	1.0002586	1,0002665	1.0002572	1.0002573

Table 3.3: Comparison of classical and relativistic Doppler widths at different temperatures for various ions in ly-alpha

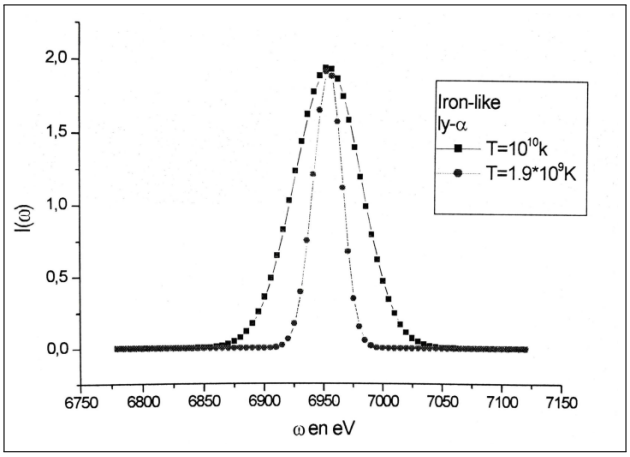

Fig 3.6: Relativistic Doppler broadening of the ly-α line of Iron-like for different temperatures

In figure 3.7, we present a comparison between the non-relativistic and relativistic Doppler widths for the Lyman-alpha line of the Cn^{+111} ion across various temperatures. The examination of the Doppler widths, both relativistic and non-relativistic, is conducted at different temperatures for the Lyman-alpha line of hydrogen-like Copernicium Cn^{+111} (see figure 3.7). Within the same table, a minor discrepancy between the two Doppler widths is observed, where the ratio specified by formula 2.33 is less than one and demonstrates an increase as the temperature rises. This observation is consistent with the findings presented in Table 3.3.

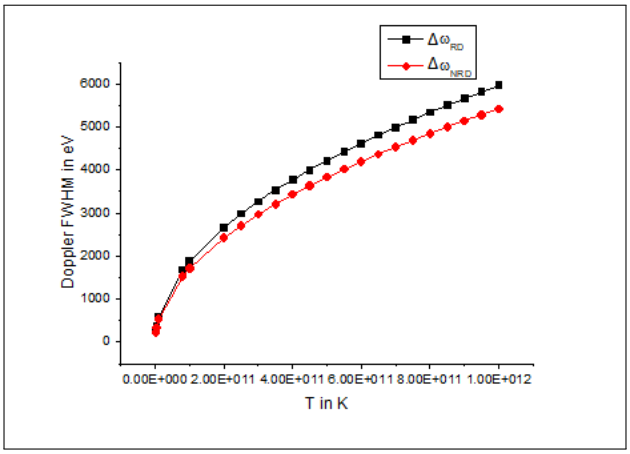

Fig 3.7: non-relativistic and relativistic Doppler width (FWHM in eV) at different temperature for ly-alpha of Copernicium Cn^{+111} and the ratio defined by formula 2.35

3.2.3 Experimental Comparison

To validate our theoretical formula against experimental results, we refer to Haines's paper [28] and examine the Full Widths at Half Maximum (FWHM) of the experimental lines (refer to figures 1 and 2 in ref. [28]). In this context, Doppler broadening predominates. Table 3.4 illustrates a numerical comparison between the theoretical formula (2.12) of FWHM ($\Delta\omega_{NRD}$) in the non-relativistic Doppler width, the relativistic width $\Delta\omega_{RD}$ (FWHM given by formula (2.33)), and the experimental FWHM ($\Delta\omega_{\text{exp}}$) of selected lines from fig 1 in ref. [28]. We selected lines based on their simplicity, avoiding those with multiple peaks. The table clearly shows the dominance of Doppler broadening, contributing up to 50% or more for all represented lines (see the last column in Table (3.4). Discrepancies arise due to numerous other broadening effects such as Stark, natural, and instrumental effects.

As another comparison, Fig. 3.8 displays the experimental measurement of the Fe He-β line (from shot Z1137ref [28]), contrasting with the relativistic Doppler broadening provided by our relativistic formula at T=300KeV. Here again, Doppler broadening emerges as the dominant factor over other mentioned broadening mechanisms.

It is important to highlight that in our calculations of theoretical widths, we have taken into account that the masses of the ions are equal to the atomic mass minus the mass of the lost electrons.

Table 3.4 illustrates a comparison between non-relativistic, relativistic Doppler FWHM, and experimental lines at a constant ionic temperature $T = 3.4813 \times 10^9$ K. Here, the transition $\omega_{0,\text{exp}}$ and the experimental FWHM $\Delta\omega_{\text{exp}}$ [20], along with our non-relativistic FWHM $\Delta\omega_{NRD}$, and our relativistic FWHM $\Delta\omega_{RD}$ are measured in eV. Notably, from

Transitions	$\omega_{0,\text{exp}}$	$\Delta\omega_{\text{exp}}$	$\Delta\omega_{RD}$	$\Delta\omega_{NRD}$	$\frac{\Delta\omega_{RD}}{\Delta\omega_{\text{exp}}}$ (%)
CrHe:2-1	5633.3	45.	33.007	32.87	73.04
CrH:2-1	5866.7	50.	34.375	34.232	68.46
FeH:2-1	6933.3	65	39.2	39.034	60.05
FeH:3-1	7867.3	80	44.48	44.292	55.36
FeHe:5-1	8433.4	52	47.681	47.48	91.30

Table 3.4: Comparison between non-relativistic, relativistic Doppler FWHM, and experimental lines at ionic temperature $T = 3.4813 \times 10^9$ K.

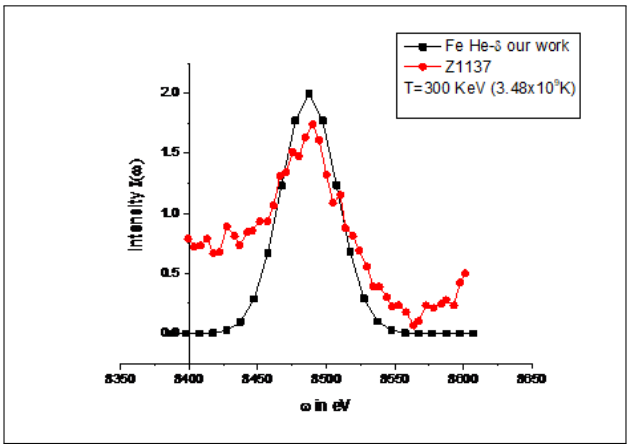

Fig 3.8: The measured of of Fe He-δ line at 8.488 keV (from shot Z1137) compared to relativistic Doppler broadening using an ion temperature of 300 keV

table 3.4, it is evident that the Fe-He:5-1 line stands out as a promising candidate for ion temperature diagnostics in plasma, given the relatively small difference between the experimental and theoretical Doppler FWHM (refer to the last column of Table 3.4). Furthermore, it's worth mentioning that there is a noticeable shift in these lines due to various factors. Additionally, asymmetry is observed in these lines (refer to figures 1-2 in [28]).

	$FeHe - \delta_{ourwork}$	$FeHe - \delta_{Z1137}$
ω_L	8464.42	8422.0874
ω_R	8510.42	8529.588
I_L	1.053563041	0.67841
I_R	1.057219702	0.55598
$A(\%)$	0.00173	-0.0992

Table 3.5: Asymmetry percentages for Figure 3.8

3.3 Stark and Doppler broadening

3.3.1 Introduction

In this section, we will conduct a comparative analysis between Doppler and Stark broadening in both classical and relativistic scenarios for $Ly-\alpha$ lines emitted by hydrogen-like ions. Additionally, we will include experimental comparisons in our investigation.

3.3.2 Stark Broadening

The Stark effect serves as one of the mechanisms responsible for spectral line broadening. It occurs when an atom, molecule, or ion emitting light into a gas is influenced by interactions with other constituents of the plasma gas, such as other atoms, molecules, ions, or electrons. The study of Stark broadening in spectral lines by plasma-charged particles has been a longstanding subject of research, continually evolving [13–16, 50–56].

The quantum treatment of Stark effect broadening is complex due to its involvement of two opposing contributions, each corresponding to the markedly different behaviors of ions and electrons. Two approximations are commonly used in the calculation of line profiles:

The quasi-static approximation arises from the movement of ions, which are much slower compared to electrons. In this approximation, the field generated by disruptive ions interacting with the emitting atom (ion) is assumed to be static. The line profile is obtained by weighting each Stark component with a distribution function of the electric micro-field. This quasi-static effect of ions, characterized by a few strong interactions, primarily affects the wings of the spectral line [55, 56].

The broadening by the impact approximation is attributed to the rapid movement of electrons, resulting in numerous collisions between interfering electrons and the emitting atom (ion). This broadening is expressed by an operator known as the electron collision operator. The theoretical study of spectral line profiles in the impact approximation has been the focus of extensive research since Baranger's papers in 1958, building upon Anderson's work from 1949 [51]. Griem [54] and Saha-Brecht [13] successfully utilized Baranger's theoretical results by adopting the impact approximation in the quasi-classical framework to compute the electron collision operator. Following these works, Professor M.T. Meftah extended the theory to the relativistic dynamics case [17]. This extension focused on Stark broadening due to electron collisions, particularly in very hot plasmas ($T \geq 10^8 K$), where this broadening is expressed by an operator called the electron collision operator. Additionally, in [57], the authors developed the relativistic collision operator, representing the broadening of isolated lines emitted by hydrogen-like ions due to collisions

with free electrons.

3.3.3 Comparison between Doppler and stark broadening

Many researches have been done to compare Doppler and Stark broadening in classical case.

In particular temperature or density conditions, one effect typically predominates the others depending on the local plasma temperature and density.

In some cases, we can ignore the others broadenings, but in others, it is preferable to take into account two or more broadenings. For example in [58], the authors have tried to present the importance of not being neglected the stark broadening in analysis of hot stars spectra in some cases where the Doppler broadening has dominated. The some for the research paper [59], even when Doppler width is greater than Stark, Stark broadening may still be significant or non-negligible in the line wings.

3.3.3.1 Classical comparison

The table 3.7, highlights the variation in Doppler and Stark widths for different spectral lines across a range of temperatures and densities. It indicates that the ratio of Doppler to Stark width varies significantly depending on the specific conditions and the nature of the spectral line. This comparison helps understand the relative contributions of Doppler and Stark broadening in different plasma environments.

This comparison provides valuable insights into the behavior of spectral lines in diverse plasma environments. and understanding the relative contributions of Doppler and Stark broadening helps characterize the physical properties of plasmas, such as temperature, density, and composition.

3.3.3.2 Relativistic Comparison

Now, we present a comparison of relativistic effects on the experimental width, relativistic Doppler width [62], and relativistic Stark width [57].

The table reveals that as the temperature increases, the ratio $\frac{\Delta\omega_D}{\Delta\omega_s}$ also increases. This indicates the significance of Doppler width, especially in classical cases where relativistic effects are not considered. Doppler broadening becomes predominant, as it is directly related to temperature. On the other hand, stark broadening is influenced by both temperature and density. Notably, with stark width, as temperature rises, stark width decreases while density increases.

In the relativistic scenario (for Cobalt), stark width decreases with increasing temperature. In this context, Doppler broadening emerges as more significant than stark broadening under certain conditions, highlighting the importance of considering both effects in plasma dynamics [57].

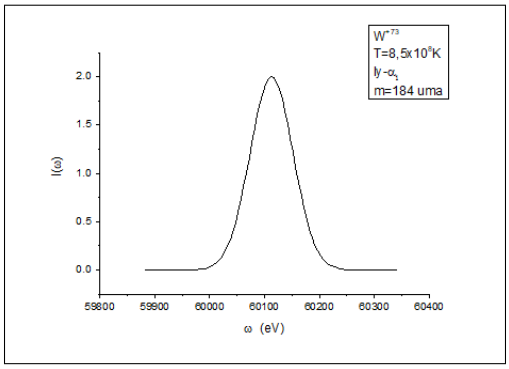

Fig 3.9: Relativistic Doppler broadening of ly-alpha line for W^{+73}

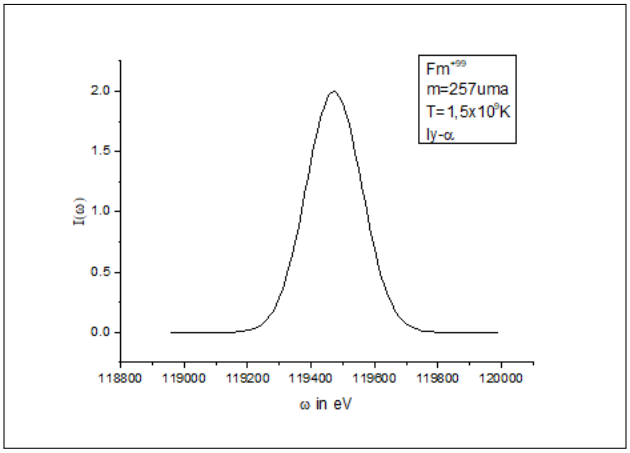

Fig 3.10: Relativistic Doppler broadening of ly-alpha line for Fm^{+99}

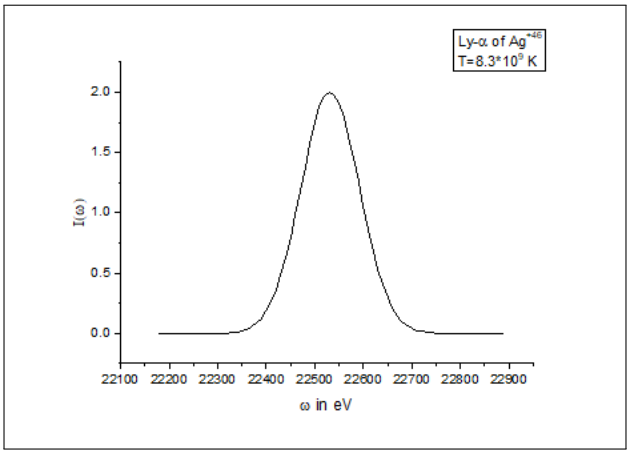

Fig 3.11: Relativistic Doppler broadening of ly-alpha line for Ag^{+46}

3.4 Conclusion

In this chapter, we conducted an analysis of the broadening effects on line profiles induced by both non-relativistic and relativistic Doppler effects. We observed significant relativistic influences on the spectral line broadening, particularly through comparisons across different hydrogen-like ions and varying temperatures of Lyman-α lines.

In the relativistic case, particularly at extremely high temperatures, the dominant broadening mechanism shifts towards the Doppler effect. This trend is prominently illustrated in Table 3.2 and Figure 3.8. Specifically, the relativistic Doppler effect introduces asymmetry in the right-hand side of the spectral line profile, as evidenced in Table 3.2 and Figures 3.5, 3.9, 3.10, and 3.11, unlike the traditional Doppler effect [28], [62].

Moreover, we conducted a comparative analysis between Doppler and Stark broadening in both classical and relativistic scenarios. In classical contexts, previous studies have extensively investigated the interplay between Doppler and Stark broadening, providing valuable insights into their relative importance under various conditions.

For the relativistic case, we referred to the work presented in [57], which provided calculations of stark width for specific hydrogen-like ions, particularly for Lyman-α lines. This allowed us to understand the nuances of stark broadening in the relativistic domain and its implications for line profile analysis.

$\lambda(A^\circ)$	$T(K^\circ)$	$Ne(cm^{-3})$	$\Delta\omega_D$	W_{MSE}	W_{fit}	W_{Cow}	W_{SCP}	W_e	$\frac{\Delta\omega_D}{\Delta\omega_s}$	ref
$Co\ II$	5000		0.01592	0.05564					0.29	
$3d^7(^4F)4s$	50000	10^{17}	0.05035	0.01760					~ 3	
$a\ ^5F_4 - 3d^7$										[60]
$(^4F)4p$										
$z^5F_4^0$										
2417.659	100000		0.07119	0.01271					~ 6	
$Co\ II$										
$3d^8F_2 - 3d^7$										
$(^4F)4p$										
$z^3F_4^0$										
2027.040	10000	2.41×10^{14}	0.01888		3.16×10^{-4}	2.50×10^{-4}			$\sim 60 - 76$	[61]
$Zn\ III$	5000		0.0149	0.0200					~ 1	
										[58]
$4s^1D - 4p^1D^o$	50000	10^{17}	0.0473	0.0141					~ 3.5	
1619.6	100000		0.0666	0.00446					~ 15	
$Xe\ VIII$	20000		0.75×10^{-2}				0.656×10^{-2}		~ 1	
										[19]
$5s^2S_{1/2.} - 5p^2P^0_{1/2}$	100000	10^{17}	0.01694				0.414×10^{-2}		~ 4	
858.6	500000		0.03788				0.141×10^{-2}		~ 27	
$Cr\ VI$										
										[59]
$4s^2S - 4p^2P^o$	400000	10^{17}	0.0897					0.0159	~ 6	
1430.0	400000		0.1268					0.00294	~ 43	

Table 3.6: Classical comaprison between classical Doppler width (FWHM) and classical stark width

$\lambda(eV)$	$T(K^\circ)$	$Ne(cm^{-3})$	$\Delta\omega_{\exp}$	$\Delta\omega_{CD}$	$\Delta\omega_{RD}$	$\Delta\omega_{LW}$	$\frac{\Delta\omega_{RD}}{\Delta\omega_{LW}}$
$Ly-\alpha$ of $FeXXVI$	3.48×10^9	10^{26}	65	39.034	39.20	12.78	~ 3
$Ly-\alpha$ of $CrXXIV$	3.48×10^9	10^{26}	50	34.232	34.375	17.36	~ 2
$Ly-\alpha$ of $CoXXIV$	1.2×10^9	10^{26}	/	24.28	24.30	11.68	~ 2
$Ly-\alpha$ of $CoXXIV$	5.1×10^9	10^{26}	/	50.062	50.097	11.334	~ 4.5

Table 3.7: Relativistic comparison between relativistic Doppler width (FWHM) and relativistic stark width

General conclusion

Spectral line-broadening effects such as natural line broadening, instrumental line broadening, Doppler broadening, electron impact broadening, and Stark broadening are all added together to produce the line's total width. Depending on the local plasma temperature and density, one effect usually dominates the others under certain temperature or density conditions, and the others are regarded as minor corrections to the dominant one. But in some cases, it is preferable to consider two broadening.

Atoms or ions that emit radiation are converted into signal sources in plasma by obeying the law of speed distribution. As a result, the radiation from these sources is affected by the Doppler effect, which causes the emission line of plasma radiation to widen. This phenomenon, known as Doppler broadening, is seen in plasma spectroscopy and has been the focus of a number of studies.

In this work, our investigation focuses on studying the impact of the relativistic Doppler effect on spectral line profiles in ultra-hot plasmas within a laboratory setting. It is important to note that the relativistic Doppler effect occurs when the emitters of radiation move at extremely high velocities, surpassing the speed of light c. Such situations are encountered in various scenarios, including laser implosion, astrophysics, and high-temperature laser technology [28], where temperatures range from 10^8 to 10^{11}K. Indeed, it is crucial to exercise caution when developing the theory of spectral line broadening in the presence of relativistic effects. Specifically, within the mentioned temperature range, the movement of emitting ions becomes highly significant, making the Doppler effect dominant. It is essential to consider the relativistic nature of the emitter's motion. Additionally, it is worth noting that the Doppler effect can manifest as a shift in the radiation or signal generated by plasma or objects undergoing global motion [38].

In this work, We've devised a new expression for relativistic Doppler broadening (relativistic case) that accounts for the emitters' possible high velocity, this means that emitters should have an appropriate velocity distribution. In contrast to the well-known conventional Gaussian, we observed an asymmetry in the Doppler broadening. Furthermore, we have derived a novel Full Width at Half Maximum (FWHM) formula specifically tailored

for the relevant profile, which differs from the FWHM formula used in the non-relativistic case [44, 62].

We also confirmed that, Stark broadening is usually negligible comparable to the Doppler broadening, where, this broadening mechanism is dominant.

Doppler broadening is generally considered to be dominant when the thermal motion of particles in a system is the primary source of line broadening. This occurs when the system is at a relatively high temperature, typically in the range of hundreds to thousands of Kelvin. At such temperatures, the random velocities of atoms or molecules result in a broad distribution of Doppler shifts, causing the spectral lines to widen.

Stark broadening, on the other hand, becomes more significant when the density of charged particles, usually electrons, is high and the electric field strength is substantial. This typically occurs in dense plasmas, such as those found in laboratory discharges, stellar atmospheres, or certain types of astrophysical objects. In these conditions, the interactions between charged particles and their electric fields lead to shifts and redistributions of energy levels, resulting in broadened spectral lines.

The dominance of Doppler broadening or Stark broadening depends on the specific characteristics of the system being studied. Generally, Doppler broadening tends to dominate at high temperatures, whereas Stark broadening becomes more significant in high-density plasmas with strong electric fields. However, it is essential to consider both mechanisms and their interplay when analyzing spectral lines to accurately interpret the physical conditions and properties of the system under investigation.

For example : if temperatures ranged from 20000 K to 500000 K, where $n_e = 10^{17} cm^{-3}$, stark broadening is dominant, it gives Lorentzian profile, but in low density, it must take the Doppler broadening into account (convolution), it gives Voigt profile, and in the range of temperature $10^8 < T < 10^{11}$K,it was found that Doppler broadening is always predominant (the relativistic case),and it gives Gaussian profile, but that Stark broadening should be taken into account or not neglected at very high densities. Here are a few examples that illustrate the dominance of Doppler broadening and Stark broadening in different systems:

1. Doppler Broadening: - When observing the spectrum of a star, the absorption lines from the stellar atmosphere exhibit significant broadening due to Doppler shifts caused by the thermal motion of atoms and molecules at high temperatures. - In the field of high-temperature plasma physics, such as in fusion experiments or astrophysical plasmas, the broadening of emission or absorption lines is predominantly governed by Doppler broadening due to the high thermal velocities of particles.

2. Stark Broadening: - In laboratory discharges, such as those used in plasma physics research, the spectral lines emitted by the plasma exhibit broadening due to the inter-

actions between electrons and the electric fields generated by the surrounding charged particles. This broadening is primarily caused by Stark effects and is used to infer plasma parameters like electron density and electric field strength. - When analyzing the spectra of white dwarf stars, the strong gravitational fields present lead to high electron densities, resulting in prominent Stark broadening of the spectral lines. This effect provides insights into the density and composition of the stellar atmospheres.

3. Combined Doppler and Stark Broadening: - In astrophysical environments such as stellar atmospheres, both Doppler broadening and Stark broadening can contribute to the observed line profiles. The broadening of spectral lines can provide information about the temperature, velocity, and density of the stellar plasma. - In laboratory fusion experiments, where high-temperature plasmas are produced, both Doppler broadening and Stark broadening occur simultaneously. The broadening of emission lines allows scientists to study the properties of the plasma, such as ion temperatures, particle densities, and the effects of electric fields.

These examples demonstrate how Doppler broadening and Stark broadening are observed in various scientific contexts and how their dominance varies depending on the specific system and its physical conditions. In our investigation, we also discovered a slight discrepancy between the two Doppler widths, namely the relativistic widths and the non-relativistic widths. This difference becomes more pronounced as the temperature rises.

Bibliography

[1] Hans-Joachim Kunze. *Introduction to plasma spectroscopy*, volume 56. Springer Science & Business Media, 2009.

[2] José A Bittencourt. *Fundamentals of plasma physics*. Springer Science & Business Media, 2013.

[3] Ian H Hutchinson. Principles of plasma diagnostics. *Plasma Physics and Controlled Fusion*, 44(12):2603–2603, 2002.

[4] Nicholas A Krall, Alvin W Trivelpiece, and KR Symon. Principles of plasma physics. *IEEE Transactions on Plasma Science*, 2(3):196–196, 1974.

[5] Wolfhard Möller. Fundamentals of plasma physics. *University of Technology Dresden*, 2014.

[6] Jean-Loup Delcroix and Abraham Bers. Physique des plasmas (vol. ii). In *Physique des plasmas (Vol. II)*. EDP Sciences, 1994.

[7] Andreas Dinklage, Thomas Klinger, Gerrit Marx, and Lutz Schweikhard. *Plasma physics: confinement, transport and collective effects*, volume 670. Springer Science & Business Media, 2005.

[8] Michel Moisan and Jacques Pelletier. *Physique des plasmas collisionnels: application aux decharges haute frequence (Collection Grenoble sciences)*. EDP sciences, 2006.

[9] Paul Gibbon. Introduction to plasma physics. *arXiv preprint arXiv:2007.04783*, 2020.

[10] Hans Griem. *Spectral line broadening by plasmas*. Elsevier, 2012.

[11] David Salzmann. *Atomic physics in hot plasmas*. Number 97. Oxford University Press, USA, 1998.

[12] Michael Zellner. Comparison of stark broadening and doppler broadening of spectral lines in dense hot plasmas. *Millersville University*, 2008.

[13] S Sahal-Bréchot. Impact theory of the broadening and shift of spectral lines due to electrons and ions in a plasma. *Astronomy and Astrophysics, Vol. 1, p. 91 (1969)*, 1:91, 1969.

[14] I de Andrés-García, A Alonso-Medina, and C Colón. Stark widths and shifts for spectral lines of sn iv. *Monthly Notices of the Royal Astronomical Society*, 455(2):1145–1155, 2016.

[15] Dejan Dojić, Miloš Skočić, Srdjan Bukvić, and Stevan Djeniže. Stark broadening measurements of al ii, al iii and he i 388.86 nm spectral lines at high electron densities. *Spectrochimica Acta Part B: Atomic Spectroscopy*, 166:105816, 2020.

[16] Dejan Dojić, Miloš Skočić, Srdjan Bukvić, and Stevan Djeniže. Experimental stark widths of mo i and mo ii spectral lines in visible region. *Journal of Physics B: Atomic, Molecular and Optical Physics*, 53(7):075001, 2020.

[17] A Naam, MT Meftah, S Douis, and S Alexiou. Spectral line broadening by relativistic electrons in plasmas: Collision operator. *Advances in Space Research*, 54(7):1242–1247, 2014.

[18] D Voslamber. Some novel concepts for spectroscopic diagnostics in tokamaks. In *AIP Conference Proceedings*, volume 328, pages 3–27. American Institute of Physics, 1995.

[19] Milan S Dimitrijević, Zoran Simić, Andjelka Kovačević, Aleksandar Valjarević, and Sylvie Sahal-Bréchot. Stark broadening of xe viii spectral lines. *Monthly Notices of the Royal Astronomical Society*, 454(2):1736–1741, 2015.

[20] Ursel Fantz. Basics of plasma spectroscopy. *Plasma sources science and technology*, 15(4):S137, 2006.

[21] Sun Mi Chung, Jeremy J Drake, Vinay L Kashyap, Li Wei Lin, and Peter W Ratzlaff. Doppler shifts and broadening and the structure of the x-ray emission from algol. *The Astrophysical Journal*, 606(2):1184, 2004.

[22] JS Wark, H He, O Renner, M Kopeckỳ, E Foerster, and Th Miβalla. Measurements of motional doppler shifts in x-rays emitted by laser-produced plasmas. *Journal of Quantitative Spectroscopy and Radiative Transfer*, 51(1-2):397–406, 1994.

[23] Z Simić, MS Dimitrijević, N Milovanović, and Sylvie Sahal-Bréchot. Stark broadening of cd i spectral lines. *Astronomy & Astrophysics*, 441(1):391–393, 2005.

[24] NI Kosarev. Influence of the doppler effect on radiative transfer in a spherical plasma under macroscopic motion of substance. *Journal of Quantitative Spectroscopy and Radiative Transfer*, 207:54–60, 2018.

[25] K Fujii, Y Takahashi, Y Nakai, D Kato, M Goto, S Morita, M Hasuo, LHD Experiment Group, et al. Visible emission spectroscopy of highly charged tungsten ions in lhd: Ii. evaluation of tungsten ion temperature. *Physica Scripta*, 90(12):125403, 2015.

[26] M Shinohara, K Fujii, D Kato, N Nakamura, M Goto, S Morita, M Hasuo, LHD Experiment Group, et al. Visible emission spectroscopy of highly charged tungsten ions in lhd: I. survey of new visible emission lines. *Physica Scripta*, 90(12):125402, 2015.

[27] Yuan-Pei Yang, Jin-Ping Zhu, and Bing Zhang. Relativistic astronomy. iii. test of special relativity via doppler effect. *The Astrophysical Journal*, 883(2):159, 2019.

[28] MG Haines, PD LePell, CA Coverdale, B Jones, C Deeney, and JP Apruzese. Ion viscous heating in a magnetohydrodynamically unstable z pinch at over 2× 10 9 kelvin. *Physical review letters*, 96(7):075003, 2006.

[29] Peter Debye and Erich Hückel. On the theory of electrolytes. i. freezing point depression and related phenomena. *Phys. Z*, 24:185–206, 1923.

[30] Douis Saïd. *Propriétés Statistiques Des Electrons Dans Un Plasma Haute Température*. PhD thesis, Université d'El Oued, 2013.

[31] G Livadiotis and DJ McComas. Electrostatic shielding in plasmas and the physical meaning of the debye length. *Journal of Plasma Physics*, 80(3):341–378, 2014.

[32] Hans R Griem. *Principles of plasma spectroscopy*. 2005.

[33] Arnold Sommerfeld. Atomic structure and spectral lines. *(No Title)*, 1923.

[34] Takashi Fujimoto and Atsushi Iwamae. *Plasma polarization spectroscopy*, volume 44. Springer, 2008.

[35] Robert D Cowan. *The theory of atomic structure and spectra*, volume 3. Univ of California Press, 2023.

[36] Daniel R Frankl. General treatment of the doppler effect in special relativity. *American Journal of Physics*, 52(4):374–375, 1984.

[37] Robert Lambourne. The doppler effect in astronomy. *Physics Education*, 32(1):34, 1997.

[38] Y-S Huang and K-H Lu. Formulation of the classical and the relativistic doppler effect by a systematic method. *Canadian journal of Physics*, 82(11):957–964, 2004.

[39] HOU Fynbo. Doppler broadened γ-lines from exotic nuclei. *Nuclear Instruments and Methods in Physics Research Section B: Beam Interactions with Materials and Atoms*, 207(3):275–282, 2003.

[40] Cristian Neipp, A Hernández, JJ Rodes, Andrés Márquez, Tarsicio Beléndez, and Augusto Beléndez. An analysis of the classical doppler effect. *European journal of physics*, 24(5):497, 2003.

[41] Christian Møller. The theory of relativity. 1972.

[42] John David Jackson. Classical electrodynamics, 1999.

[43] Seiji Zenitani. Loading relativistic maxwell distributions in particle simulations. *Physics of Plasmas*, 22(4), 2015.

[44] Mohammed Tayeb Meftah, Hadda Gossa, Kamel Ahmed Touati, Keltoum Chenini, and Amel Naam. Doppler broadening of spectral line shapes in relativistic plasmas. *Atoms*, 6(2):16, 2018.

[45] C Stehlé, D Gilles, and AV Demura. Asymmetry of stark profiles: The microfield point of view. *The European Physical Journal D-Atomic, Molecular, Optical and Plasma Physics*, 12(2):355–367, 2000.

[46] John F Seely. Gigagauss magnetic field measurements using zeeman broadening of ne-like transitions in highly charged ions. *Review of Scientific Instruments*, 92(5), 2021.

[47] Young-Sea Huang, Juang-Han Chiue, Yi-Chi Huang, and Te-Chih Hsiung. Relativistic formulation for the doppler-broadened line profile. *Physical Review A*, 82(1):010102, 2010.

[48] Laurent Schwartz. Théorie des distributions à valeurs vectorielles. i. In *Annales de l'institut Fourier*, volume 7, pages 1–141, 1957.

[49] WR Johnson and Gerhard Soff. The lamb shift in hydrogen-like atoms, 1 z 110. *Atomic Data and Nuclear Data Tables*, 33(3):405–446, 1985.

[50] Hans R Griem, Alan C Kolb, and KY Shen. Stark broadening of hydrogen lines in a plasma. *Physical Review*, 116(1):4, 1959.

[51] PHILIP W Anderson. Pressure broadening in the microwave and infra-red regions. *Physical Review*, 76(5):647, 1949.

[52] Michel Baranger. Simplified quantum-mechanical theory of pressure broadening. *Physical Review*, 111(2):481, 1958.

[53] Michel Baranger. General impact theory of pressure broadening. *Physical Review*, 112(3):855, 1958.

[54] Hans R Griem and KY Shen. Stark broadening of hydrogenic ion lines in a plasma. *Physical Review*, 122(5):1490, 1961.

[55] HR Griem, M Baranger, AC Kolb, and G Oertel. Stark broadening of neutral helium lines in a plasma. *Physical Review*, 125(1):177, 1962.

[56] M Baranger. Atomic and molecular processes ed dr bates (new york: Academic). 1962.

[57] K Arif, MT Meftah, K Chenini, S Douis, Y Ben Nana, and H Gossa. Contribution of liénard–wiechert potential to the broadening of spectral lines by electron collisions in plasmas. *Physics of Plasmas*, 29(9), 2022.

[58] Abeer Almodlej, Zlatko Majlinger, Nabil Ben Nessib, Milan S Dimitrijević, and Vladimir A Srećković. Impact of stark broadening on co ii spectral line modelling in hot stars. *The European Physical Journal D*, 75(4):141, 2021.

[59] MS Dimitrijević, Z Simić, and S Sahal-Bréchot. On the stark broadening of cr vi spectral lines in astrophysical plasma. In *Journal of Physics: Conference Series*, volume 810, page 012021. IOP Publishing, 2017.

[60] Zlatko Majlinger, Milan S Dimitrijević, and Vladimir A Srećković. Stark broadening of co ii spectral lines in hot stars and white dwarf spectra. *Monthly Notices of the Royal Astronomical Society*, 496(4):5584–5590, 2020.

[61] Milan S Dimitrijević and Magdalena D Christova. Stark broadening of zn iii spectral lines. *Universe*, 8(8):430, 2022.

[62] H Gossa, MT Meftah, K Chenini, DE Zenkhri, B Amieur, and H Guerrida. The spectral line asymmetry of the doppler effect in relativistic plasmas. *Europhysics Letters*, 139(2):20001, 2022.

Appendix

tocchapterAppendix

The relativistic Doppler profile

$$\begin{aligned} I(\omega) &= <\delta(\omega-\omega(\beta))>_{Juttner-Maxwell} = \int W_{J-M}(\beta)d\beta\delta(\omega-\omega(\beta)) \\ &= \frac{1}{2\pi}\int_{-\infty}^{+\infty} du \int_0^{2\pi}\int\int W_{J-M}(\beta)d\beta \exp(iu(\omega-\omega(\beta)))\sin\theta d\theta d\phi \\ &= \int_{-\infty}^{+\infty} du \int\int W_{J-M}(\beta)d\beta \exp(iu(\omega-\omega(\beta)))\sin\theta d\theta \\ &= \int_{-\infty}^{+\infty} du\exp(iu\omega)\int\int W_{J-M}(\beta)d\beta\exp(-iu\omega(\beta)))\sin\theta d\theta \end{aligned}$$

We have

$$W_{J-M}(\beta)d\beta = \frac{\gamma^5\beta^2}{\alpha K_2\left[\lambda\right]}\exp(-\gamma\lambda)d\beta$$

So we can write

$$\begin{aligned} I(\omega) &= \int_{-\infty}^{+\infty}\exp(iu\omega)du\int_0^1\int_0^\pi \frac{\gamma^5\beta^2}{\alpha K_2\left[\frac{1}{\alpha}\right]}\exp(-\frac{\gamma}{\alpha})\exp(-iu\omega_0\gamma(1-\beta\cos\theta))d\beta\sin\theta d\theta \\ I(\omega) &= \frac{1}{\alpha K_2\left[\frac{1}{\alpha}\right]}\int_{-\infty}^{+\infty}\exp(iu\omega)du\int_0^1\gamma^5\beta^2\exp(-\frac{\gamma}{\alpha})\exp(-iu\omega_0\gamma)d\beta\int_0^\pi\exp(iu\omega_0\gamma\beta\cos\theta)\sin\theta d\theta \end{aligned}$$

After making the integral over θ, we obtain:

$$
\begin{aligned}
I(\omega) &= \frac{1}{i\alpha\omega_0 K_2\left[\frac{1}{\alpha}\right]} \int_{-\infty}^{+\infty} \exp(iu\omega)\frac{du}{u} \\
&\quad \times \int_0^1 \gamma^4\beta \exp(-\frac{\gamma}{\alpha}) \exp(-iu\omega_0\gamma)(\exp(iu\omega_0\gamma\beta) - \exp(-iu\omega_0\gamma\beta)))d\beta
\end{aligned}
$$

$$
\begin{aligned}
I(\omega) &= \frac{1}{i\alpha\omega_0 K_2\left[\frac{1}{\alpha}\right]} \int_{-\infty}^{+\infty} \exp(iu\omega)\frac{du}{u} \\
&\quad \times \left[\int_0^1 \gamma^4\beta \exp(-\frac{\gamma}{\alpha}) \exp(iu\omega_0(\beta-\gamma))d\beta - \int_0^1 \gamma^4\beta \exp(-\frac{\gamma}{\alpha}) \exp(-iu\omega_0(\gamma+\beta)d\beta\right] \\
&= I_1(\omega) - I_2(\omega)
\end{aligned}
$$

Where :

$$
\begin{aligned}
I_1(\omega) &= \frac{1}{i\alpha\omega_0 K_2\left[\frac{1}{\alpha}\right]} \int_{-\infty}^{+\infty} \exp(iu\omega)du \int_0^1 \gamma^4\beta \exp(-\frac{\gamma}{\alpha}) \exp(iu\omega_0(\beta-\gamma))d\beta \\
I_2(\omega) &= \frac{1}{i\alpha\omega_0 K_2\left[\frac{1}{\alpha}\right]} \int_{-\infty}^{+\infty} \exp(iu\omega)du \int_0^1 \gamma^4\beta \exp(-\frac{\gamma}{\alpha}) \exp(-iu\omega_0(\beta+\gamma))d\beta
\end{aligned}
$$

We have also:

$$
\begin{aligned}
\gamma^2 &= \frac{1}{1-\beta^2} \\
\gamma d\gamma &= \frac{\beta d\beta}{(1-\beta^2)^2} = \gamma^4\beta d\beta \\
\beta d\beta &= \frac{d\gamma}{\gamma^3}
\end{aligned}
$$

So :

$$
\begin{aligned}
I_1(\omega) &= \frac{1}{i\alpha\omega_0 K_2\left[\frac{1}{\alpha}\right]} \int_0^1 \gamma d\gamma \exp(-\frac{\gamma}{\alpha}) \int_{-\infty}^{+\infty} \exp(iu\omega_0(\beta - \gamma + \frac{\omega}{\omega_0}))\frac{du}{u} \\
I_2(\omega) &= \frac{1}{i\alpha\omega_0 K_2\left[\frac{1}{\alpha}\right]} \int_0^1 \gamma d\gamma \exp(-\frac{\gamma}{\alpha}) \int_{-\infty}^{+\infty} \exp(iu\omega_0(-\beta - \gamma + \frac{\omega}{\omega_0}))\frac{du}{u}
\end{aligned}
$$

We can write :

$$
\begin{aligned}
I_1(\omega) &= \frac{1}{i\alpha\omega_0 K_2\left[\frac{1}{\alpha}\right]} \int_0^1 \gamma d\gamma \exp(-\frac{\gamma}{\alpha}) \int_{-\infty}^{+\infty} \exp(iu(a+b))\frac{du}{u} \\
I_2(\omega) &= \frac{1}{i\alpha\omega_0 K_2\left[\frac{1}{\alpha}\right]} \int_0^1 \gamma d\gamma \exp(-\frac{\gamma}{\alpha}) \int_{-\infty}^{+\infty} \exp(iu(a-b))\frac{du}{u}
\end{aligned}
$$

Where $a = \omega_0(\frac{\omega}{\omega_0} - \gamma)$ and $b = \omega_0\beta$

$$
\begin{aligned}
I(\omega) &= \frac{1}{i\alpha\omega_0 K_2\left[\frac{1}{\alpha}\right]} \int_0^1 \gamma d\gamma \exp(-\frac{\gamma}{\alpha}) \int_{-\infty}^{+\infty} \left[\exp(iu(a+b)) - \exp(iu(a-b))\right]\frac{du}{u} \\
I(\omega) &= \frac{1}{i\alpha\omega_0 K_2\left[\frac{1}{\alpha}\right]} \int_0^1 \gamma d\gamma \exp(-\frac{\gamma}{\alpha}) \int_{-\infty}^{+\infty} \left[2i\cos au \sin bu - 2\sin au \sin bu\right]\frac{du}{u}
\end{aligned}
$$

The second sinus integral is zero, so

$$
\begin{aligned}
I(\omega) &= \frac{1}{i\alpha\omega_0 K_2\left[\frac{1}{\alpha}\right]} \int_0^1 \gamma d\gamma \exp(-\frac{\gamma}{\alpha}) \int_{-\infty}^{+\infty} 2i\cos au \sin bu\frac{du}{u} \\
I(\omega) &= \frac{4}{\alpha\omega_0 K_2\left[\frac{1}{\alpha}\right]} \int_0^1 \gamma d\gamma \exp(-\frac{\gamma}{\alpha}) \int_{0}^{+\infty} \cos au \sin bu\frac{du}{u}
\end{aligned}
$$

After making the integral over u, we obtain:

$$
I(\omega) = \frac{\pi}{\alpha\omega_0 K_2\left[\frac{1}{\alpha}\right]} \int_0^1 \gamma d\gamma \exp(-\frac{\gamma}{\alpha}) \left(sign(a+b) - sign(a-b)\right)
$$

Where

$$\begin{aligned} a &= \omega_0(\frac{\omega}{\omega_0}-\gamma) \\ b &= \omega_0\beta \\ a+b &= \omega_0(\frac{\omega}{\omega_0}-\gamma+\beta)=\omega_0(\frac{\omega}{\omega_0}-\gamma+\frac{\sqrt{\gamma^2-1}}{\gamma}) \\ a-b &= \omega_0(\frac{\omega}{\omega_0}-\gamma-\beta)=\omega_0(\frac{\omega}{\omega_0}-\gamma-\frac{\sqrt{\gamma^2-1}}{\gamma}) \end{aligned}$$

The simplified relativistic Doppler profile

$$I(\varpi)=\frac{\lambda}{2K_2\left[\lambda\right]}\exp(-\lambda)\int_1^\infty \gamma d\gamma\exp(-\lambda\gamma)\times\Big(sign(\varpi-\gamma+\sqrt{\gamma^2-1})-sign(\varpi-\gamma-\sqrt{\gamma^2-1})\Big)$$

Making the integral over for λ

$$\begin{aligned} I(\varpi)\int\frac{2K_2\left[\lambda\right]}{\lambda}d\lambda &= \int\int_1^\infty \gamma d\gamma\exp(-\lambda\gamma) \\ &\quad\times\Big(\mathrm{sign}(\varpi-\gamma+\sqrt{\gamma^2-1})-\mathrm{sign}(\varpi-\gamma-\sqrt{\gamma^2-1})\Big)\,d\lambda \\ I(\varpi)\int\frac{2K_2\left[\lambda\right]}{\lambda}d\lambda &= -\int_1^\infty d\gamma\exp(-\lambda\gamma)\times\Big(\mathrm{sign}(\varpi-\gamma+\sqrt{\gamma^2-1})-\mathrm{sign}(\varpi-\gamma-\sqrt{\gamma^2-1})\Big) \\ I(\varpi)\int\frac{2K_2\left[\lambda\right]}{\lambda}d\lambda &= -\int_1^\infty d\gamma\exp(-\lambda\gamma)\times\mathrm{sign}(\varpi-\gamma+\sqrt{\gamma^2-1}) \\ &\quad+\int_1^\infty d\gamma\exp(-\lambda\gamma)\times\mathrm{sign}(\varpi-\gamma-\sqrt{\gamma^2-1}) \end{aligned}$$

We have from $(uv)^{'}=u'v+v'u$
$\int v'u=uv-\int u'v$
Let's assume $u=sign(\varpi-\gamma+\sqrt{\gamma^2-1})$ and $v'=\exp(-\lambda\gamma)d\gamma$
So

$$\begin{aligned} I(\varpi)\int\frac{2K_2\left[\lambda\right]}{\lambda}d\lambda &= \Big(\frac{1}{\lambda}\exp(-\lambda\gamma)\times sign(\varpi-\gamma+\sqrt{\gamma^2-1})\Big)_1^\infty \\ &\quad+\frac{1}{\lambda}\int\exp(-\lambda\gamma)(\frac{2\gamma}{\sqrt{\gamma^2-1}}-2)\delta(\varpi-\gamma+\sqrt{\gamma^2-1})d\gamma \\ &\quad\Big(-\frac{1}{\lambda}\exp(-\lambda\gamma)\times sign(\varpi-\gamma-\sqrt{\gamma^2-1})\Big)_1^\infty \\ &\quad-\frac{1}{\lambda}\int\exp(-\lambda\gamma)(-\frac{2\gamma}{\sqrt{\gamma^2-1}}-2)\delta(-\varpi-\gamma+\sqrt{\gamma^2-1})d\gamma \end{aligned}$$

$$= -\frac{2}{\lambda}\int_1^\infty d\gamma \exp(-\lambda\gamma)$$
$$\times \left(\left(\frac{\gamma}{\sqrt{\gamma^2-1}} - 1 \right) \delta(\varpi - \gamma + \sqrt{\gamma^2-1}) \right.$$
$$\left. + \left(\frac{\gamma}{\sqrt{\gamma^2-1}} + 1 \right) \delta(-\varpi + \gamma + \sqrt{\gamma^2-1}) \right)$$

Delta Dirac function properties

$$\delta(f(x)) = \frac{\delta(x - x_0)}{|f'(x_0)|}$$

We put

$$\begin{aligned}
f(\gamma) &= \varpi - \gamma - \sqrt{\gamma^2-1} \\
f'(\gamma) &= -1 - \frac{\gamma}{\sqrt{\gamma^2-1}} \\
f'(\gamma_0) &= -1 - \frac{\gamma_0}{\sqrt{\gamma_0^2-1}} \\
g(\gamma) &= -\varpi + \gamma + \sqrt{\gamma^2-1} \\
g'(\gamma) &= 1 + \frac{\gamma}{\sqrt{\gamma^2-1}} \\
g'(\gamma_0) &= 1 + \frac{\gamma_0}{\sqrt{\gamma_0^2-1}} \\
\delta(\varpi - \gamma + \sqrt{\gamma^2-1}) &= \frac{\delta(\gamma - \gamma_0)}{\frac{\gamma_0}{\sqrt{\gamma_0^2-1}} - 1} \\
\delta(-\varpi + \gamma + \sqrt{\gamma^2-1}) &= \frac{\delta(\gamma - \gamma_0)}{1 + \frac{\gamma_0}{\sqrt{\gamma_0^2-1}}}
\end{aligned}$$

So

$$
\begin{aligned}
I(\varpi)\int \frac{2K_2[\lambda]}{\lambda}d\lambda &= -\frac{2}{\lambda}\int_1^\infty d\gamma \exp(-\lambda\gamma)\left((\frac{\gamma}{\sqrt{\gamma^2-1}}-1)\frac{\delta(\gamma-\gamma_0)}{\frac{\gamma_0}{\sqrt{\gamma_0^2-1}}-1}+(\frac{\gamma}{\sqrt{\gamma^2-1}}+1)\frac{\delta(\gamma-\gamma_0)}{1+\frac{\gamma_0}{\sqrt{\gamma_0^2-1}}}\right)\\
I(\varpi)\int \frac{2K_2[\lambda]}{\lambda}d\lambda &= -\frac{2}{\lambda}\int_1^\infty d\gamma \exp(-\lambda\gamma)\left((\gamma\Gamma-1)\frac{\delta(\gamma-\gamma_0)}{\gamma_0\Gamma_0-1}+(\gamma\Gamma+1)\frac{\delta(\gamma-\gamma_0)}{1+\gamma_0\Gamma_0}\right)\\
\Gamma &= \frac{1}{\sqrt{\gamma^2-1}};\Gamma_0=\frac{1}{\sqrt{\gamma_0^2-1}}
\end{aligned}
$$

We have $\Gamma=\left(\sqrt{\gamma^2-1}\right)^{-1/2}$

$$
\begin{aligned}
I(\varpi)\int \frac{2K_2[\lambda]}{\lambda}d\lambda &= -\frac{2}{\lambda}\int_1^\infty d\gamma \exp(-\lambda\gamma)\left((\gamma\Gamma-1)\frac{\delta(\gamma-\gamma_0)}{\gamma_0\Gamma_0-1}+(\gamma\Gamma+1)\frac{\delta(\gamma-\gamma_0)}{1+\gamma_0\Gamma_0}\right)\\
&= -\frac{2}{\lambda}\int_0^\infty d\gamma \exp(-\lambda\gamma)\delta(\gamma-\gamma_0)\left(\frac{(\gamma\Gamma-1)}{\gamma_0\Gamma_0-1}+\frac{(\gamma\Gamma+1)}{1+\gamma_0\Gamma_0}\right)\\
&= -\frac{4}{\lambda}\int_1^\infty d\gamma \exp(-\lambda\gamma)\delta(\gamma-\gamma_0)\left(\frac{\gamma\Gamma\gamma_0\Gamma_0-1}{(\gamma_0\Gamma_0)^2-1}\right)\\
&= -\frac{4}{\lambda}\int_1^\infty d\gamma \exp(-\lambda\gamma)\delta(\gamma-\gamma_0)f(\gamma);f(\gamma)=\frac{\gamma\Gamma\gamma_0\Gamma_0-1}{(\gamma_0\Gamma_0)^2-1}\\
&= -\frac{4}{\lambda}\exp(-\lambda\gamma_0)
\end{aligned}
$$

So

$$
\begin{aligned}
I(\varpi)\int \frac{2K_2[\lambda]}{\lambda}d\lambda &= -\frac{4}{\lambda}\exp(-\lambda\gamma_0)\\
I(\varpi)\frac{2K_2[\lambda]}{\lambda} &= -4(-\exp(-\lambda\gamma_0)\frac{1}{\lambda^2}-\gamma_0\frac{1}{\lambda}\exp(-\lambda\gamma_0))\\
I(\varpi) &= \frac{2}{K_2[\lambda]}\exp(-\lambda\gamma_0)(\frac{1}{\lambda}+\gamma_0)\\
I(\varpi) &= \frac{2}{K_2[\lambda]}\exp(-\lambda\frac{\varpi^2+1}{2\varpi})(\frac{1}{\lambda}+\frac{\varpi^2+1}{2\varpi})
\end{aligned}
$$

For find FWHM

We have

$$\begin{aligned} I(1+\frac{\Delta\varpi}{2}) &= \frac{1}{2}I(1) \\ I(\omega_0+\frac{\Delta\omega}{2}) &= \frac{1}{2}I(\omega_0) \\ \varpi &= \frac{\omega}{\omega_0} \end{aligned}$$

So

$$\begin{aligned} \frac{1}{2}\frac{2}{K_2[\lambda]}\exp(-\lambda)(\frac{1}{\lambda}+1) &= \frac{2}{K_2[\lambda]}\exp(-\lambda\frac{\left(1+\frac{\Delta\varpi}{2}\right)^2+1}{2\left(1+\frac{\Delta\varpi}{2}\right)})(\frac{1}{\lambda}+\frac{\left(1+\frac{\Delta\varpi}{2}\right)^2+1}{2\left(1+\frac{\Delta\varpi}{2}\right)}) \\ \frac{1}{2}\exp(-\lambda)(\frac{1}{\lambda}+1) &= \exp(-\Lambda)(\frac{1}{\lambda}+\frac{\Lambda}{\lambda}); \Lambda = \lambda\frac{\left(1+\frac{\Delta\varpi}{2}\right)^2+1}{2\left(1+\frac{\Delta\varpi}{2}\right)} \\ \frac{1}{2}\frac{(\frac{1}{\lambda}+1)}{(\frac{1}{\lambda}+\frac{\Lambda}{\lambda})}\exp(-\lambda) &= \exp(-\Lambda) \\ \exp(-\Lambda) &= \frac{1}{2}\frac{1+\lambda}{1+\Lambda}\exp(-\lambda) \end{aligned}$$

let's assume $\Lambda_0(\lambda)$ the solution of last equation so

$$\Delta\varpi_{RD} = 2\sqrt{\left(\frac{\Lambda_0(\lambda)}{\lambda}\right)^2+1}$$

And

$$\Delta\omega_{RD} = \omega_0\Delta\varpi_{RD} = 2\omega_0\sqrt{\left(\frac{\Lambda_0(\lambda)}{\lambda}\right)^2+1}$$